Simulation study of wettability alteration enhanced oil recovery during co-current spontaneous imbibition

Pål Ø. Andersen[1,2,], Sameer Ahmed[1]*
1 Department of Energy Resources, University of Stavanger
2 The National IOR Centre of Norway
** Corresponding author (pal.andersen@uis.no)*

Abstract

Naturally fractured reservoirs are highly dependent on capillary forces to recover hydrocarbons during water injection. Water can spontaneously imbibe and expel oil if positive capillary forces exist; purely counter-current if all sides of the matrix blocks are exposed to water; and predominantly co-current with some counter-current production if the blocks are exposed to water and oil simultaneously. The latter is referred to as a co-current spontaneous imbibition (SI) setup. Wettability alteration (WA) has been identified as a key mechanism to improve oil recovery from naturally fractured reservoirs, however almost all experimental and modelling studies on WA during SI have focused on counter-current SI. Our review indicates limited systematic experimental work on co-current SI using nonzero initial saturation, mixed wettability or WA processes and This modelling study will investigate enhanced oil recovery by WA during co-current SI where a brine with a general WA component imbibes and causes the system to become more water-wet.

We model a 1D oil-saturated core exposed to water at one end (inlet) and oil at the other end (outlet), thus facilitating co-current SI. The core is initially preferentially (not strongly) oil-wet with low SI potential. The component is both transported by the imbibing brine and diffuses towards the imbibition front. Adsorption of the component is assumed to improve the water-wetness of the porous medium and hence the SI potential. The model is parameterized using consistent capillary pressure and relative permeabilities from previous history matching of brine-dependent porous disc experiments.

The behavior of co-current SI at mixed-wet state is examined and compared to that of literature strongly water-wet behavior. Both secondary and tertiary enhanced recovery by SI with WA component is then considered in the simulations. Important parameters such as mobility ratio (as via oil viscosity), capillary back pressure, WA component concentration, adsorption and time of WA component exposure are investigated.

Under mixed-wet conditions, favorable and unfavorable mobility ratios do not limit oil production as can be the case for strongly wetted media at unfavorable mobility ratio. This is due to oil preserving mobility at all obtained saturations. A third or more of the total production was counter-current, which is high compared to strongly wetted media. It was shown that half the oil could be produced counter-currently as an upper limit. High oil mobility is preserved in the twophase region near the inlet and was found to ensure a high minimum fraction of counter-current production. Twice as much of the incremental oil from WA was produced counter-currently as co-currently, explained by increased oil relative permeability in the WA affected inlet region. Sensitivity analysis revealed that an opposite shift would reduce the incremental counter-current production despite raised local capillary forces. Capillary back pressure resists oil production at the inlet without limiting water from imbibing. As a result, capillary back pressure had significant impact on co-current SI simulations with fixed and changing wettability.

The trends discovered in this study, both for mixed-wet and wettability alternating systems, are hoped to inspire future experimental measurements.

Keywords: co-current spontaneous imbibition; enhanced oil recovery; wettability alteration; molecular diffusion; adsorption

Nomenclature

Roman	
a	Adsorbed concentration, -
c	Concentration, -
D	Diffusion coefficient, m^2/s
f_w	Water fractional flow function, -
F	Wettability interpolation function, -
K	Absolute permeability, m^2
k_d	Distribution coefficient, -
k_{ri}	Relative permeability, -
L	System length, m
m	Diffusion cementation exponent, -
n	Diffusion saturation exponent, -
n_i	Corey exponent, -
P_c	Capillary pressure, Pa
P_{cbo}	Capillary back pressure to oil at the inlet, Pa
p_i	Phase pressure, Pa
q_a, q_b, q_c	J-function parameters, Pa
r_a, r_b	J-function parameters, -
RF^{co}	Co-current recovery factor, -
RF^{cou}	Counter-current recovery factor, -
RF^{tot}	Total recovery factor, -
s_i	Phase saturation, -
s_{ir}	Residual phase saturation, -
S_w	Normalized water saturation, -
t	Simulation time, s
u_i	Darcy phase velocity, m/s
Greek	
λ_i	Phase mobility, -
μ_i	Phase viscosity, Pa s
ϕ	Porosity, -
Indices	
c	Capillary
i	Phase
j	Index for wetting dataset
o	Oil
T	Total
w	Water
Abbreviations	
EOR	Enhanced oil recovery
MW	Mixed-wet
pow	Preferentially oil-wet

pww	Preferentially water-wet
SI	Spontaneous imbibition
SWW	Strongly water-wet
WA	Wettability alteration

1. Introduction

Spontaneous imbibition (SI) is a phenomenon in which non-wetting fluid is displaced spontaneously by wetting fluid due to capillary forces. SI plays an important role in naturally fractured reservoirs where a dense and highly permeable fracture network causes the advective forces to not be effective in displacing oil (referred to as the non-wetting fluid in this work) from the matrix blocks (Aronofsky et al. 1958; Firoozabadi 2010; Andersen 2019). Matrix wettability is an important factor which governs the extent at which SI can take up wetting fluid (assumed to be water in this work), and the rate at which this occurs (Zhou et al. 2000). The more the system prefers the wetting phase, the higher both these parameters tend to be. If the matrix is preferentially oil-wet, naturally fractured reservoirs produced by water injection may hence acquire a low economic oil recovery factor. Imbibition rate is also controlled by fluid mobilities, initial saturation, block vs fracture shape, dimensions, intrinsic properties and saturation functions (Mattax and Kyte 1962; Xie and Morrow 2001; Zhou et al. 2002; Fischer and Morrow 2006; Mason et al. 2009).

Wettability alteration (WA) can be applied to improve the SI potential and imbibition rate as demonstrated by several experimental and simulation works. Altering the oil-brine-rock system wettability has been linked to modifying brine salinity or composition (RezaeiDoust et al. 2009; Dang et al. 2013; Qiao et al. 2014; Mahani et al. 2015; Xie et al. 2019), adding surfactants (Standnes and Austad 2000; Delshad et al. 2009; Joonaki et al. 2016), nanoparticles (Suleimanov et al. 2011; Nazari Moghaddam et al. 2015) or carbon dioxide (Seyyedi et al. 2015). In addition to the previous factors; imbibition rate during WA depends on composition, concentration, adsorption and diffusion (Stoll et al. 2008; Andersen et al. 2015).

Notably, most experimental works attempting to characterize WA are performed either applying the Amott test where a core is surrounded by brine on all sides or by conventional core flooding (forced displacement). In both cases the brine composition is usually changed (relative to the connate water composition) or the temperature is changed in order to perturb the initial thermochemical equilibrium defining the initial wetting state. At the same time, it is well documented that SI can take place not only counter-currently, but also co-currently. A pure counter-current SI flow regime can take place when the matrix block is homogeneous, symmetric, all (open) sides are exposed to water and capillary forces dominate (Mason and Morrow 2013). However, co-current flow will be important especially when the matrix block is exposed to different phases on different surfaces. Bourbiaux and Kalaydjian (1990) exposed a SWW Vosges sandstone sample to water on one side with all other sides closed and compared that with when the sample was exposed to oil on an additional side. Not only did oil production happen faster, and predominantly co-currently in the latter case, but they determined by simulation that significantly higher relative permeability functions were needed to model in the co-current mode. Ca 3 % of the produced oil was from counter-current production in the co-current setup. Pooladi-Darvish and Firoozabadi (2000) found by simulation that for SWW media typically 5-10% of recoverable oil would be produced counter-currently when a sample was exposed to water on one side and oil on the other, and the rest co-currently, irrespective of sample length. Their results also predicted production to be faster with the oil-exposed side open, than if it was closed (counter-current flow). Standnes (2004) investigated imbibition rate for SWW samples covered to different extent by water and oil and found that if the area exposed to oil was larger than that exposed to water, the imbibition would go faster than if all the area was exposed to water. Higher end recovery was observed from samples recovered in co-current

mode compared to counter-current mode. 5-10% of the recovered oil was produced counter-currently.

Every matrix block in the reservoir will only gradually be exposed to water, which occurs when the injected water, or water rising from a supporting aquifer, gradually advances or rises in the fracture network. Hence, co-current SI is the first flow regime every matrix block encounters upon water contact. As the injected water (such as seawater) often is not in chemical equilibrium with the reservoir it is reasonable to expect that co-current SI of brine causing WA and hence EOR is an occurring event in the reservoir.

Significant gravitational forces can also induce a net co-current flow even under symmetric exposure to water (Xie and Morrow 2001; Qiao et al. 2018). Schechter et al. (1994) correlated this behavior with the Bond number, which expresses the ratio between gravitational and capillary forces. Standnes and Austad (2000) showed that surfactant could displace oil counter-currently from all sides of a strongly oil-wet core by WA, while another surfactant slowly displaced oil vertically by gravity. Imbibition by gravitational forces with all open sides exposed to water is by some authors called co-current imbibition (Babadagli 2000, 2005), but is a different mechanism than the purely capillary pressure driven flow studied in this work. Karimaie et al. (2006) studied imbibition into a long vertical SWW core due to water rising around it. At fast water rise counter-current production was seen visually as oil droplets entering the water. More efficient recovery and higher ultimate recovery was seen at low rates where co-current SI took place or high density difference where gravity enhanced co-current flow.

The co-current SI setup is in the following defined by a horizontally oriented core (to eliminate gravity effects) exposed to water on one side (inlet), oil on the other side (outlet) and its radial sides closed. Under those conditions co-current SI is enabled if positive capillary forces exist, i.e. the core is mixed-wet or strongly water-wet. Co-current oil production will occur at the outlet, but also, counter-current oil production can occur at the inlet. For this setup, mobility ratio has been investigated for SWW systems. It is indicated that a favorable mobility ratio allows to produce the mobile oil efficiently (little mobile oil behind the water front) in a close to piston-like manner and little counter-current production: Washburn (1921) showed theoretically and by experiment that water could displace air by SI into a capillary tube in piston-like fashion with square root of time recovery. Akin et al. (2000) imbibed water displacing air or oil co-currently in SWW sandstone and diatomite. In the former they saw square root of time recovery, while it was more irregular in the latter. No counter-current production was reported although that could be related to the use of a filter at the inlet and the vertical inclination of the core. At favorable mobility ratio Haugen et al. (2014) tested SWW cores from chalk and sandstone using fluids with close to equal viscosities (~1 cP) but varied the core lengths. Similar recovery profiles, mainly varying in time scale were observed with all mobile oil recovered when the water reached the outlet. No more than ~5% counter-current recovery was reported although the total recovery reached ~55% (both lithologies). Meng et al. (2016) varied the wetting phase viscosity from similar to that of the non-wetting phase and upwards. Both quartz and glass packs were used as porous medium. In both cases the same end recovery was obtained regardless of wetting phase viscosity although the recovery differed between the media. No counter-current production was reported.

However, for unfavorable mobility ratios, low displacement efficiency causes much mobile oil to be left when the water reaches the outlet. When the water reaches the outlet, the water saturation can build up and drastically reduce the oil mobility at the outlet and limit further co-current production. Counter-current production can be significant. Haugen et al. (2015) performed co-current SI with oil viscosity 83 and 137 cP while brine was the wetting phase (1.1 cP). The counter-current recovery was 0.23 in the high viscosity case, of similar magnitude as the co-current recovery of 0.37 (0.12 and ~0.4 for the 83 cP case, respectively). Hamidpour et al. (2015) presented an experimental study of co-current SI using reservoir core

samples cleaned and burned to obtain water-wet conditions. They varied the brine to oil viscosity ratio between 0.04 and 16. They claimed that all the tests resulted in square root of time recovery profiles irrespective of viscosity ratio, but did not require the fitted curves to start at zero recovery at initial time. They reported that a 'small portion' of the oil production was counter-current, less at higher water viscosity. Meng et al. (2017) observed that the apparent end recovery reduced drastically with increased non-wetting viscosity (from 0.01 to 100 cP) and fixed wetting viscosity of ~1 cP and linked this to viscosity dependent microscopic sweep. However, by interpretation of the experiments by simulation this phenomenon was explained by Andersen et al. (2019a) as caused by the mobility restriction at the outlet. The latter work also presented experiments on high permeability sand packs where the viscosity of the non-wetting phase was varied from 0.01 to 70 cP and brine was wetting phase. They showed that mobility restrictions at the inlet (caused by a filter) could strongly affect the overall mobility of the system and determine the recovery profiles. Both latter works observed increased counter-current production with non-wetting viscosity towards ~0.12 at the highest non-wetting viscosity.

The capillary back pressure refers to the added resistance for a phase to be produced from a porous medium into a surrounding phase, such as when oil expelled during SI forms a bubble that must detach from the surface. Unsal et al. (2007) studied this phenomenon with capillary tubes and noted that the creation of such bubbles slowed down the counter-current production significantly. Simple piston-like displacement models for co-current SI were presented by Haugen et al. (2014) and Fernø et al. (2015) and used to calculate representative relative permeability values ahead of and behind the front, the front capillary pressure and the inlet capillary back pressure. Experiments with different viscosity ratios were interpreted to map different points of the saturation functions. Andersen et al. (2019a) used full numerical simulation to interpret the role of saturation functions and the capillary back pressure for experimental data. The analysis was extended to include the interplay with viscous coupling in Andersen et al. (2019b). Viscous coupling accounts for the drag force between the flowing phases and can effectively result in lower relative permeabilities during counter-current flow than co-current flow (Standnes et al. 2017). It was shown that this effect could result in low counter-current production, a similar response as from a high capillary back pressure. Andersen (2020a) presented an analytical model for co-current SI using Buckley-Leverett saturation profiles instead of piston-like displacement assumptions. He demonstrated that the mobility of the imbibing saturation profile compared to the initial mobility of the system determines whether the imbibition rate will increase, decrease or stay constant.

Our review indicates that most of the existing research related to co-current SI has been conducted on SWW media. That is natural due to the simplicity of core preparation whereby an outcrop core with nonpolar oil and a brine can be applied with little consideration of rock, brine and oil composition, temperature and aging time, as is needed if mixed-wet (MW) conditions are applied. SWW conditions are however not considered representative reservoir conditions and are therefore not used for enhanced oil recovery (EOR) assessments. They are mainly used for exploring the role of parameters not related to wettability, such as physical and geometrical properties and general multiphase flow behavior. For EOR purposes by WA, MW conditions are used, but there seems to be no studies considering the impact of MW state on co-current SI compared to SWW state and accordingly no research where EOR during co-current SI is performed.

MW state is here defined in the sense introduced by Salathiel (1973) where the largest pores are oil-wet and the smallest pores are water-wet. Such a condition is established when the initially water-wet geological reservoir is invaded by hydrocarbons. Capillary forces resist invasion in the small pores thus remaining water-wet, while oil then resides in the large pores where polar oleic components attach to the surface making them oil-wet. Such a wettability

condition is believed to be the most representative in the reservoirs and is established in the lab by introducing oil into initially water-saturated core plugs and letting them age. A majority of the considered studies (Standnes 2004; Haugen 2014, 2015; Hamidpour 2015; Meng et al. 2016, 2017; Andersen 2019a) also applied fully hydrocarbon saturated cores at initial state, a simplifying step that does not allow MW conditions. On macroscale wettability is reflected in relative permeability and capillary pressure (Anderson 1987a,b). The MW condition is seen in especially the capillary pressure curve which then crosses the saturation axis between the lowest and highest mobile water saturation. In other words, both water and oil can be drawn into the core spontaneously by capillary forces. The water saturation where the capillary pressure is zero is the highest saturation possible to obtain by SI. In pore scale modeling the MW state can be represented by the distribution of contact angles, i.e. a porous medium with more water-wet state has a greater distribution of pores having low contact angles compared to one that is less water-wet (Behbahani and Blunt 2005). On macro-scale more water-wetness is indicated by a higher potential for water to imbibe spontaneously (Zhou et al. 2000; Karimaie et al. 2006) and hence the imbibing water saturation will be closer to the highest mobile saturation. Enhanced recovery during SI is achieved by increasing the imbibing water saturation, i.e. making the medium more water-wet.

This study presents simulation results for co-current SI at mixed-wet conditions, where the role of capillary back pressure, viscosity ratio and enhanced oil recovery by WA are in focus. This is done to contribute to new knowledge on co-current SI considering MW media and EOR. The findings and hypotheses of this study may hopefully inspire experimental works to further expand the research in this area. Some main questions we address are:

- How does co-current SI take place in MW systems?
- Is the fraction of counter-current production low, similar to SWW systems?
- Is WA able to improve both co-current and counter-current recovery?
- How does capillary back pressure affect co-current SI at MW conditions and during WA?
- How does WA component transport affect the SI process?

The paper is structured as follows: 1) A summary of the mathematical model and its assumptions. 2) Input data to the model including saturation functions at different wetting states. 3) Results and discussion based on model simulations are presented. First, we present recovery behavior during SI at fixed wetting state. We then consider secondary EOR, where WA occurs from the start by imbibition of brine carrying WA component. Then tertiary EOR is considered, where brine composition is changed from preferentially oil-wet (*pow*) to more water wet after some time of production. 4) Finally, the paper is summarized by conclusions.

2. Mathematical model

A 1D core is considered which is open for flow from two sides only at $x = 0$ (inlet) and $x = L$ (outlet). The setup is presented in **Figure 1**, where the x-axis is aligned along the core. The core is exposed to water at the inlet and oil at the outlet. Such a setup facilitates co-current SI of water from the inlet provided that positive capillary pressure exists. Co-current oil production will occur at the outlet while counter-current oil production will occur at the inlet. The phases water (w) and oil (o) are described by their saturations s_i and pressures p_i (i=w, o). The core is assumed homogenous regarding porosity ϕ and absolute permeability K. The rock and fluids are incompressible and immiscible and the system is isothermal.

Initially, the core is assumed uniformly mixed-wet with low water-wetness. The saturation where the capillary pressure is zero is denoted $s_{w,eq}$ and is hence close to the initial saturation s_{wi}. The imbibing brine can contain a wettability alteration (WA) component with concentration c. Adsorption of this component changes the wettability towards higher water-wetness. The initial wetting state will be referred to as preferentially oil-wet (*pow*). This state

can be any mixed-wet state or even a strongly oil-wet state, but for our purposes WA will make the system more water-wet compared to that state. Similarly, the most water-wet state that can be obtained under the system of investigation will be referred to as preferentially water-wet (pww). This is mainly relative to the initial state and can refer to a mixed-wet or strongly water-wet state. Two reference saturation function sets measured experimentally in the literature will be used to denote the pow and pww states. Other wetting states will be generated from interpolation. We consider processes with saturation and concentration increasing monotonously such that there is no reversal in the saturation functions or adsorption.

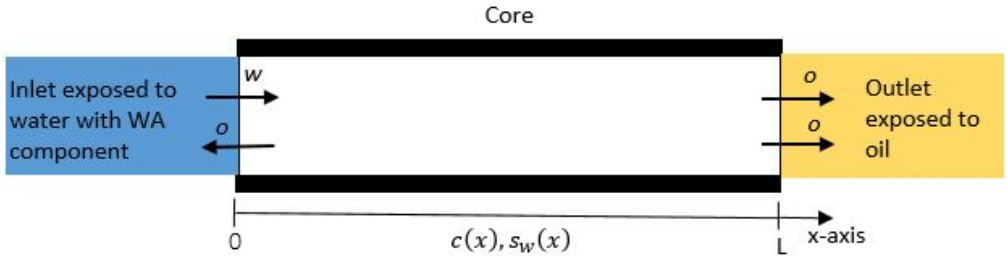

Figure 1 Illustration of the model. The core is exposed to water at the inlet (left) and oil at the outlet (right). Oil is produced in counter-current mode at the inlet and co-current mode at the outlet during the SI process.

Equations for immiscible and incompressible flow of water (w) and oil (o) under negligible gravity effects are given by (Chen et al. 2006):

$$\phi \partial_t s_w = -u_T \partial_x f_w - K \partial_x (\lambda_o f_w \partial_x P_c), \tag{1}$$

$$\partial_x u_T = 0, \tag{2}$$

where the following terminology has been applied:

$$u_T = -K(\lambda_T \partial_x p_w - \lambda_w \partial_x P_c), \tag{3}$$

$$\lambda_T = \lambda_o + \lambda_w, \qquad f_w = \frac{\lambda_w}{\lambda_T}, \qquad \lambda_i = \frac{k_{ri}}{\mu_i}, \qquad (i = o, w) \tag{4}$$

u_T is the total Darcy flux, f_w water fractional flow function, λ_i phase mobilities defined by the ratio of relative permeability k_{ri} and viscosity μ_i. $P_c(s_w) = p_o - p_w$ is the imbibition capillary pressure function. The mechanism of dynamic WA was included by adding a component to the system transported in the water phase by advection, adsorption and molecular diffusion:

$$\partial_t \big(\phi s_w c + a(c)\big) = -\partial_x (u_T f_w c) - \partial_x (K \lambda_o f_w c \partial_x P_c) + \partial_x (D \partial_x c), \tag{5}$$

$$D = D_{bulk} \phi^m s_w^n, \qquad D_{bulk} = D_0 \frac{\mu_{w,ref}}{\mu_w} \frac{T}{T_{ref}}, \tag{6}$$

$$a(c) = k_d c. \tag{7}$$

The molecular diffusion coefficient D is based on a bulk diffusion coefficient D_0 measured at reference conditions (*ref*) and corrected for solvent viscosity μ_w and temperature T to the considered conditions, giving a bulk coefficient D_{bulk}. In the porous medium the diffusion is reduced due to navigation through the tortuous pore space and water in presence of oil as indicated by the cementation and saturation exponents m, n. This correction gives the final expression for D. The adsorption is assumed linear with brine concentration as given by a constant distribution coefficient k_d (Appelo and Postma 2005). Similar equations have been applied describing sorbent transport during co- and counter-current SI at fixed wettability (Schmid et al. 2011), fracture-matrix flow with counter-current SI and WA (Andersen et al. 2015) and core flooding with capillary end effects and WA (Andersen 2020b).

The WA takes place by interpolation of the critical saturations and the normalized saturation functions, as described in the following. An interpolation parameter F is used to denote the extent of WA, where $F = 0$ means no WA (the *pow* set applies) and $F = 1$ means full WA (the *pww* set applies). In this work F is a linear function of concentration between

predefined concentration values c_{min} and c_{max} corresponding to the mentioned respective wetting states.

$$F = \frac{c - c_{min}}{c_{max} - c_{min}}, \tag{8}$$

Interpolated residual saturations are defined:

$$s_{wr} = s_{wr}^{pow} + F\left(s_{wr}^{pww} - s_{wr}^{pow}\right), \tag{9}$$

$$s_{or} = s_{or}^{pow} + F\left(s_{or}^{pww} - s_{or}^{pow}\right), \tag{10}$$

This is used to give a common normalized saturation S_{wn}^{*}:

$$S_{wn}^{*} = \frac{s_w - s_{wr}}{1 - s_{or} - s_{wr}}, \tag{11}$$

which is used to find corresponding absolute saturations $s_w^{pow,*}$, $s_w^{pww,*}$ in the mobile saturation range of the original curve sets:

$$s_w^{pow,*} = s_{wr}^{pow} + \left(1 - s_{or}^{pow} - s_{wr}^{pow}\right)S_{wn}^{*}, \tag{12}$$

$$s_w^{pww,*} = s_{wr}^{pww} + \left(1 - s_{or}^{pww} - s_{wr}^{pww}\right)S_{wn}^{*}, \tag{13}$$

The three saturation functions in each of the two saturation function sets are evaluated at their respective saturations $s_w^{pow,*}, s_w^{pww,*}$ and the function values are then interpolated by F to give effective saturation functions depending on both concentration (due to WA) and saturation:

$$k_{rw}(s_w, c) = k_{rw}^{pow}\left(s_w^{pow,*}\right) + F\left[k_{rw}^{pww}\left(s_w^{pww,*}\right) - k_{rw}^{pow}\left(s_w^{pow,*}\right)\right], \tag{14}$$

$$k_{ro}(s_w, c) = k_{ro}^{pow}\left(s_w^{pow,*}\right) + F\left[k_{ro}^{pww}\left(s_w^{pww,*}\right) - k_{ro}^{pow}\left(s_w^{pow,*}\right)\right], \tag{15}$$

$$P_c(s_w, c) = P_c^{pow}\left(s_w^{pow,*}\right) + F\left[P_c^{pww}\left(s_w^{pww,*}\right) - P_c^{pow}\left(s_w^{pow,*}\right)\right], \tag{16}$$

2.1. Saturation function correlations

The capillary pressure P_c and relative permeability functions k_{ri} representative of fixed wetting states (*pow* and *pww*) are given by parameterizing correlations from Andersen et al. (2017a) and Brooks and Corey (1966):

$$P_c^j(s_w) = \frac{q_a^j}{1 + r_a^j S_w} - \frac{q_b^j}{1 + r_b^j(1 - S_w)} + q_c^j, \tag{17}$$

$$k_{rw}^j(s_w) = k_{rw}^{*,j}(S_w)^{n_w^j}, \tag{18}$$

$$k_{ro}^j(s_w) = k_{ro}^{*,j}(1 - S_w)^{n_o^j}, \tag{19}$$

$$S_w^j = \frac{s_w - s_{wr}^j}{1 - s_{or}^j - s_{wr}^j}, \qquad \left(s_{wr}^j < s_w < 1 - s_{or}^j\right). \tag{20}$$

In the above the index j refers to either the *pow* or *pww* dataset. q_a^j, q_b^j, q_c^j are in units of pressure, where the two former are required to be nonnegative. r_a^j, r_b^j are dimensionless. S_w^j is scaled water saturation such that values ranging from 0 to 1 are obtained between the critical saturations s_{ir}^j for the considered wetting state. $k_{ri}^{*,j}$ are end point relative permeabilities, while n_i^j are Corey exponents.

2.2. Initial and boundary conditions

The core initially has critical water saturation and minimum WA component concentration (this assumes the *pow* wetting state initially):

$$s_w(x, t = 0) = s_{wr}, \qquad c(x, t = 0) = c_{min}. \tag{21}$$

However, if the *pww* wetting state is assumed initially (as in some examples), a uniform concentration of c_{max} would be assumed instead.

The inlet boundary is defined by exposure to water with a specified WA component concentration (that can be changed at given times), a zero water pressure, and a capillary back pressure to oil P_{cbo} that can be positive or zero:

(22) $$s_w(x=0,t)=1, \qquad c(x=0,t)=c_{imb}(t), \qquad p_w(x=0,t)=0,$$

(23) $$P_c(x=0^-,t)=\min\left(P_c\left(s_w(x=0^+,t),c(x=0^+,t)\right),P_{cbo}\right).$$

Mathematically, the back pressure corresponds to a constant oil pressure boundary when the matrix oil pressure is higher than the back pressure, while it corresponds to a zero oil pressure gradient if the matrix pressure is lower than the back pressure. The effect of increasing $P_{cbo} > 0$ is to reduce any positive oil pressure gradient at the inlet towards zero which reduces counter-current production of oil. It does not affect the final production since water and oil have zero pressure at the inlet and outlet, respectively creating a driving force until the capillary pressure of the system is zero. Hence, the production will shift to co-current.

The outlet is exposed to oil with zero oil pressure. The water pressure is discontinuous at this boundary and follows from the capillary pressure relation:

(24) $$s_w(x=L,t)=0, \qquad p_w(x=L^-,t)=-P_c\left(s_w(x=L^-,t),c(x=L^-,t)\right).$$

2.3. Numerical solution

The simulations were performed using IORCoreSim (Lohne 2013), a core scale simulation software developed by the National IOR Centre of Norway. The system was modelled as 1D using 100 cells in the axial direction using a Black Oil Model description for the fluids as immiscible and incompressible phases with the WA agent dissolved only in the water phase, capable to adsorb, here linearly, with concentration and change the multiphase flow functions all as described in the outlined equations of the model section. We refer to Lohne (2013) for details regarding the numerical discretization of the equations. In addition to the fine grid, convergence was ensured by limiting saturation changes to small values ($\Delta s_w = 0.002$) between calculation steps and using frequent report times.

2.4. Oil recovery

The oil recovery factor (RF) is reported as the volume fraction produced of the oil initially in place $V_{o,init}$; separated into the part produced at the outlet side (co-current recovery RF^{co}), the part produced at the inlet side (counter-current recovery RF^{cou}) and the overall production (total recovery RF^{tot}):

(25) $$RF^{co}(t)=\frac{V_{o,prod}^{outlet}(t)}{V_{o,init}}=\frac{\int_{t'=0}^{t}u_T(x=L,t)dt}{L\phi(1-s_{w0})},$$

(26) $$RF^{tot}(t)=\frac{V_{o,ip}(t)}{V_{o,init}}=\frac{\frac{1}{L}\int_{x=0}^{L}[s_w(x,t)-s_{w0}]dx}{(1-s_{w0})},$$

(27) $$RF^{cou}(t)=RF^{tot}(t)-RF^{co}(t).$$

Particularly, RF^{co} is based on the volume oil produced at the outlet $V_{o,prod}^{outlet}(t)$ found by integrating the oil flux at the outlet side (which equals the total flux), while the total recovery is calculated using the volume oil in place $V_{o,ip}(t)$ as found by integrating the saturation distribution. The volume produced at the inlet (counter-currently) corresponds to their difference.

3. Results and discussion

3.1. Input data

Capillary pressure and relative permeability input functions are shown in **Figure 2** as obtained by mathematical interpretation (Andersen et al. 2017b) of porous disk experiments on outcrop chalks at Ekofisk reservoir conditions (Ahsan et al. 2012); 130 C. Experiments were conducted at two mixed-wet states, using the same crude oil and aging procedure, but different brine composition (1.1 mol/L NaCl giving a more oil-wet state and 0.37 mol/L Na_2SO_4 giving a more water-wet state). For the considered tests, the same brine was used as both formation water and

imbibing brine. Parameters based on the experimental conditions are presented in **Table 1** to define the base case of our study. The initial saturation, permeability, porosity and viscosity values were rounded for illustrative purposes and some core-to-core variation. A system length of 10 cm was selected arbitrarily. Input parameters for the two sets of saturation functions are listed in **Table 2**.

For simplicity, we report concentration of WA agent with normalized values such that the highest value corresponding to the *pww* set is $c_{max} = 1$ (which could be 0.37 mol/L Na_2SO_4), while the minimum concentration of $c_{min} = 0$ would correspond to 1.1 mol/L NaCl. The *pow* and *pww* curves are plotted together with interpolated curves for different concentration values in **Figure 2**. Note that only the saturation range where positive capillary pressure may exist (0.05 to ca 0.45) has been plotted since other saturations will not be obtained during the SI process. The saturations $s_{w,eq}^{pow}, s_{w,eq}^{pww}$ where capillary pressure is zero for the two reference states are clearly indicated and correspond to the highest saturation possibly obtained by SI under that wetting state. The curves reflect a trend reported by McPhee et al. (2015); that increased wetting of a given phase is reflected in lower relative permeability of that phase, and vice versa. Further, increased water-wetness is reflected by more positive capillary pressures and increased saturation where the capillary pressure is zero.

Megawati et al. (2013) measured sulfate adsorption onto chalk at 130 C with Na_2SO_4, (i.e. same conditions as in Ahsan et al. (2012)), and noted a sulfate effluent concentration delay of ~0.7 pore volumes compared to inert tracer. Strand et al. (2006) used seawater with different concentrations of sulfate and saw ~0.2 PV delay at room temperature (sulfate adsorbs less at lower temperature but it also depends on brine composition). Assuming linear adsorption, we select a distribution coefficient of $k_d = 1$ giving a delay of 1 PV, comparable to the results by Megawati et al. (2013).

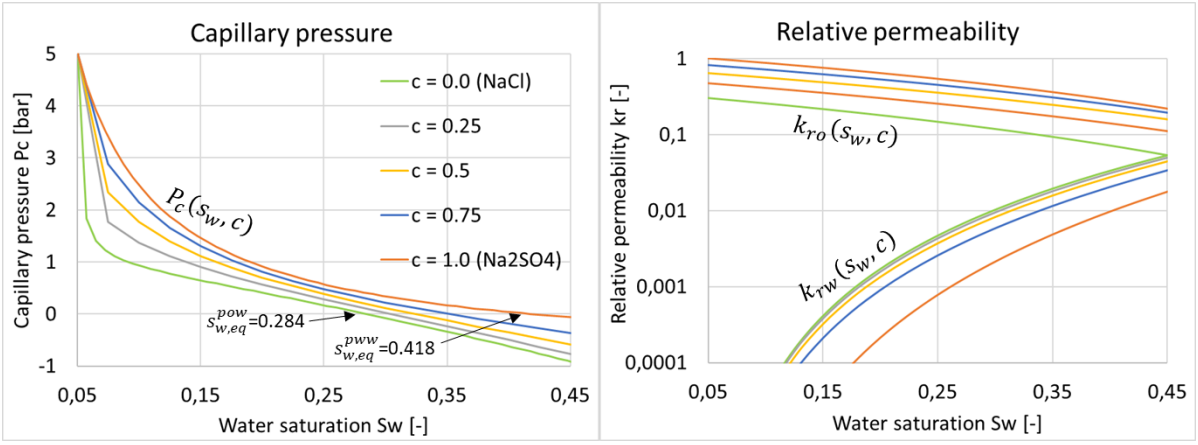

Figure 2 Capillary pressure (left) and relative permeability (right) plotted against water saturation for different concentrations. Zero concentration (light blue) corresponds to the *pow* set as measured when NaCl brine was the wetting phase, while concentration equal 1 (red curve) corresponds to the *pww* set as measured when Na_2SO_4 brine was the wetting phase. The plots are focused at the saturation range where positive capillary pressures are obtained.

Table 1 Reference input parameters.

Parameter	Values	Parameter	Values	Parameter	Values	Parameter	Values
L	10 cm	$c_{min} = c_0$	0	m	1.6	T	403 K
K	1 mD	c_{max}	1	n	2.0	T_{ref}	293 K
ϕ	0.45	$\mu_w(130°C)$	0.25 cP	D_0	$10^{-9}\ m^2/s$	k_d	1
s_{w0}	0.05	$\mu_o(130°C)$	1.0 cP	μ_{ref}	1 cP	P_{cbo}	0 bar

Table 2 Saturation function input parameters for the correlations (17) to (19).

Parameters	s_{wr}	s_{or}	k_{rw}^*	k_{ro}^*	n_w	n_o	q_a	q_b	q_c	r_a	r_b
pow	0.05	0.15	0.6	0.3	3.5	2.5	4.05	11.9	7.57	371	0.798

							bar	bar	bar		
pww	0.05	0.2	0.3	1.0	4.5	2.0	5.91 bar	5.91 bar	5 bar	11.2	0

In the following sections we investigate parameters that are considered important for co- (or counter-) current SI: mobility ratio (Haugen et al. 2014, 2015; Meng et al. 2016, 2017), capillary back pressure (Haugen et al. 2014; Fernø et al. 2015; Andersen et al. 2019a,b), wettability / saturation functions (Zhou et al. 2000), and parameters important for EOR by WA: diffusive/adsorptive component transport, concentration (Stoll et al. 2008; Andersen et al. 2015) and the time of initiating EOR. We refer to the literature review for details. These parameters are central in the various terms and boundary conditions of the model (1) to (24).

3.2. Behavior at fixed wetting state

First we consider how the *pow* system, using reference input parameters given in **Table 1**, behaves with fixed wetting state. To see the effect of varied mobility ratio we vary oil viscosity from its base value of 1 cP by factors of 10 up to 1000 cP, while keeping the water viscosity at 0.25 cP. The corresponding oil recovery trends are presented in **Figure 3**. For all viscosity cases the SI process progresses steadily towards the same final recovery of ~0.25. This corresponds exactly to the condition where the capillary pressure becomes zero, namely at $s_{w,eq}^{pow} = 0.284$ (see **Figure 2**, left) giving ultimate recovery $RF^{tot} = \frac{0.284-0.05}{1-0.05} = 0.246$. Increased oil viscosity increases the time for total recovery to stabilize from ~12 d to 500 d. In all cases, counter-current recovery has a very significant contribution with $RF^{cou} = 0.1$ for the lowest oil viscosity and increasing to 0.12 for the highest viscosity; ~45% of the total production. The corresponding co-current recovery is $RF^{co} = 0.15$ and 0.13.

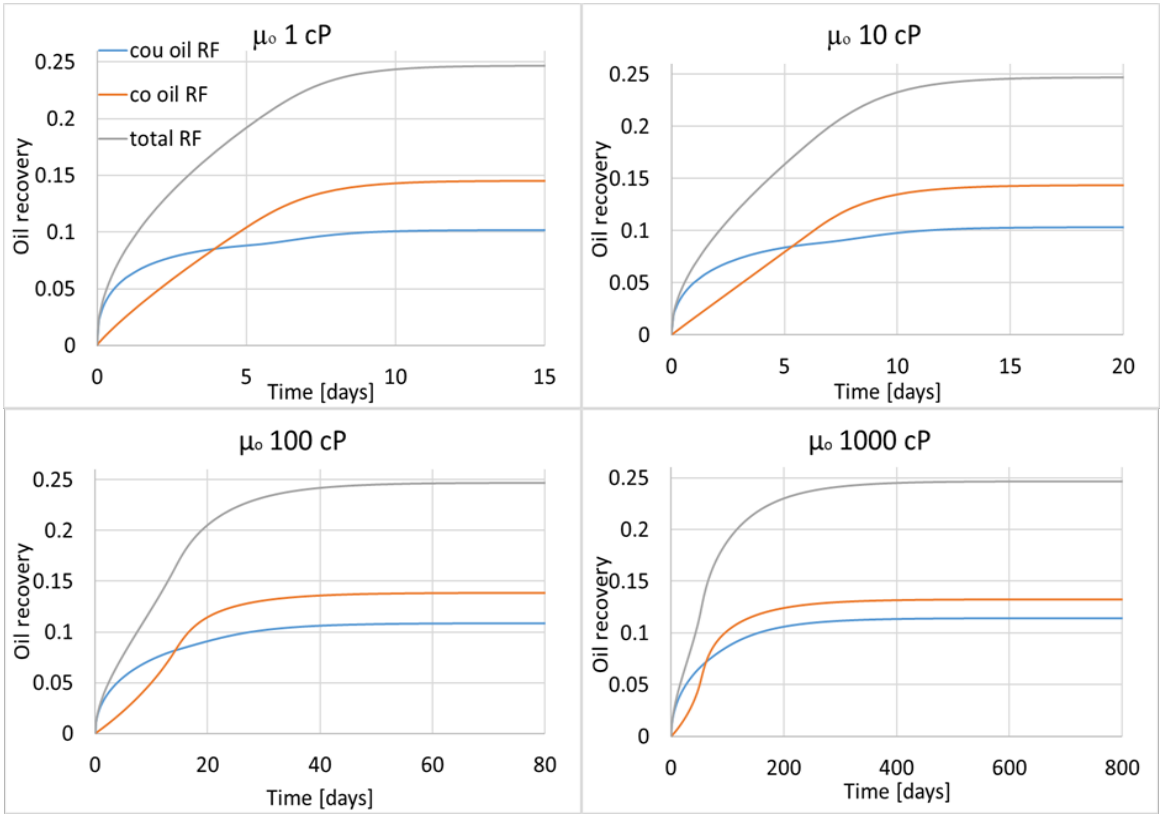

Figure 3 Recovery vs time at fixed *pow* state for different oil viscosities. Reference parameters were used.

Considering the *pww* case we have $s_{w,eq}^{pww} = 0.418$ giving a maximum recovery of 0.387. Recovery behavior for different oil viscosities is displayed in **Figure 4**. Again, for all viscosity ratios the maximum recovery is steadily approached, although the end production may appear lengthier than for the pow case, see especially for high viscosities. The end co-current recovery is highest for 1 cP oil viscosity with a value of 0.24 and decreases to 0.22 for the 1000 cP oil viscosity. Similarly, the end counter-current recovery increases with oil viscosity from 0.14 to 0.17, respectively. Also, the *pww* case demonstrates a significant counter-current production, ~40% of the total. Increased counter-current production with less favorable mobility ratio (higher oil viscosity) has been reported experimentally by Haugen et al. (2015), Meng et al. (2017) and Andersen et al. (2019a) for SWW media. If oil has low mobility it may have an easier flowpath out the inlet in multiphase flow with mobile water than towards the outlet. As the water front travels further from the inlet this will change. Note also that counter-current production dominates over co-current at early times in the examples. The former flow mode has a square root of time behavior, while co-current recovery may be linear (1 cP and 10 cP) or accelerating from a slow rate (100 cP and 1000 cP) and thus needs time to 'catch up'. This has also been observed in the aforementioned references, but with a lower counter-current fraction of the total production.

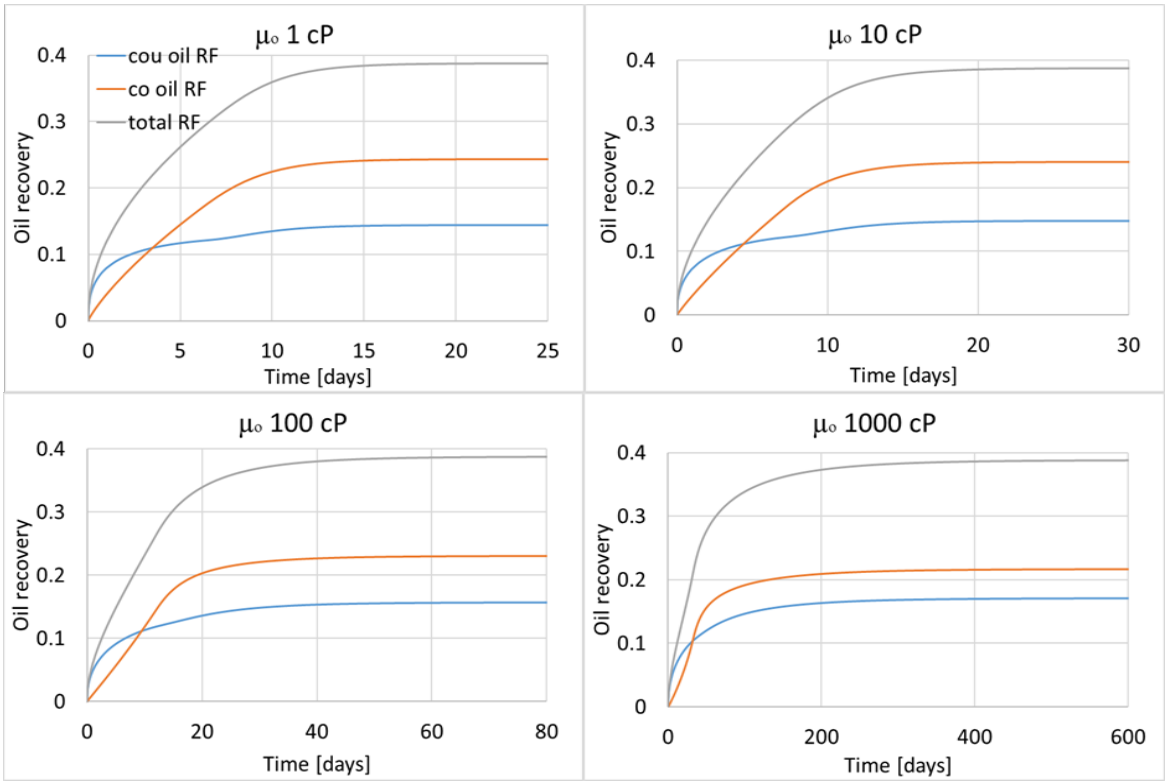

Figure 4 Recovery vs time at fixed *pww* state for different oil viscosities. Reference parameters were used.

Water saturation profiles along the core (from inlet to outlet) are shown for the *pow* and *pww* cases in **Figure 5** and **Figure 6**, respectively. For the *pow* cases, the profiles are shown when the total recovery is 0.05, 0.10, 0.15 and 0.20, while for the *pww* cases, total recovery is shown when the total recovery is 0.05, 0.10, 0.20 and 0.30. The specific times are indicated.

The profiles are in all cases relatively smooth with no sharp fronts, despite that the considered low saturation range represents favorable mobility ratios (oil has high mobility and water has low mobility). This is due to the strong capillary diffusion term which both causes counter-current production and smooths out steep saturation gradients. Some similarity can be seen with Buckley-Leverett behavior (Buckley and Leverett 1942) where the profiles can be

approximated by those of forced displacement; e.g. favorable viscosity ratios give steeper saturation gradients. This approximation was pointed out for strongly water-wet media by Mason and Morrow (2013) and Andersen et al. (2019a). With increased oil viscosity the forward moving water profiles displaces oil less efficiently: there is more oil behind the water saturation front at a given recovery and it takes more time to reach the same level of recovery (same color graph). When the water reaches the outlet, the outlet water saturation rises. For low oil viscosity cases the saturations along the core seems to increase while maintaining the negative saturation gradient. On the other hand, for high oil viscosity cases the outlet saturation rises more than the preceding saturations and a U-shaped saturation profile develops which gradually rises towards $s_{w,eq}$. In SWW media such an increased saturation at the outlet would lead to a strong reduction in the oil mobility there and the co-current imbibition rate (Andersen et al. 2019a). As seen for these cases with MW media (**Figure 3** and **Figure 4**), no drastic reduction of the imbibition rate takes place when the water reaches the outlet since the imbibing end saturation $s_{w,eq}$ is far from the saturation where oil loses mobility $1 - s_{or}$. This also explains why there is no apparent viscosity dependence on remaining oil saturation as observed by Meng et al. (2017) for SWW media where significantly less oil was recovered at increased non-wetting phase viscosity.

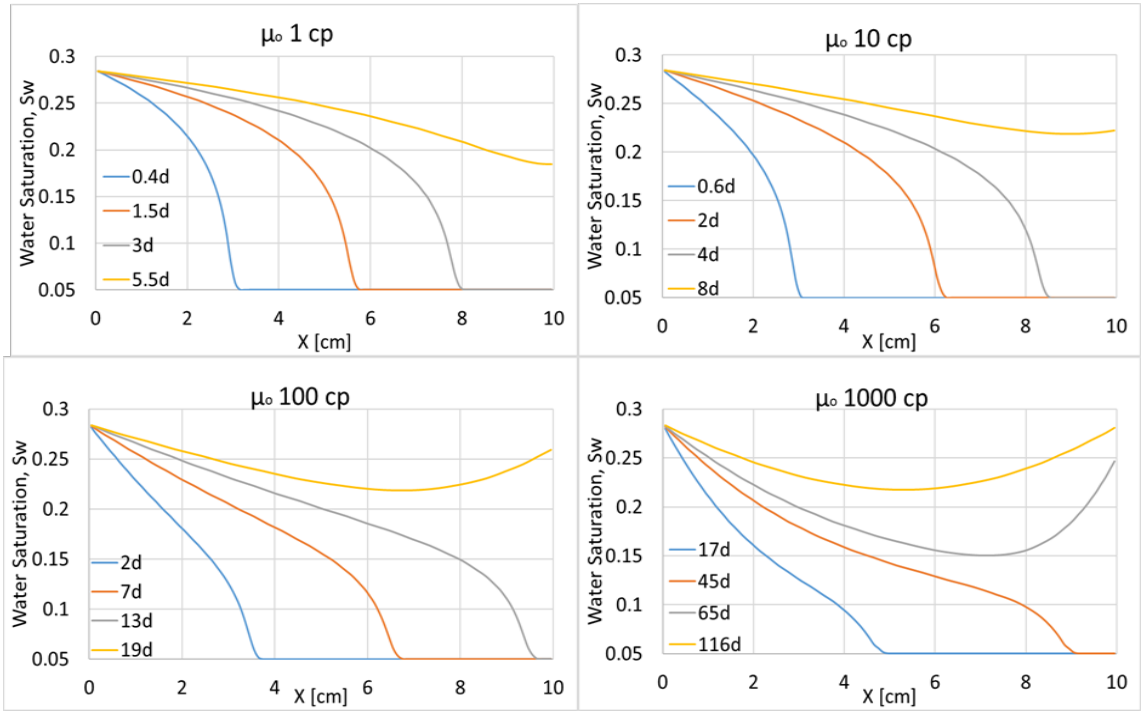

Figure 5 Water saturation profiles during SI under *pow* conditions, displayed when RF^{tot} = 0.05 (blue), 0.10 (orange), 0.15 (grey) and 0.20 (yellow) for different oil viscosities. The absolute times are indicated.

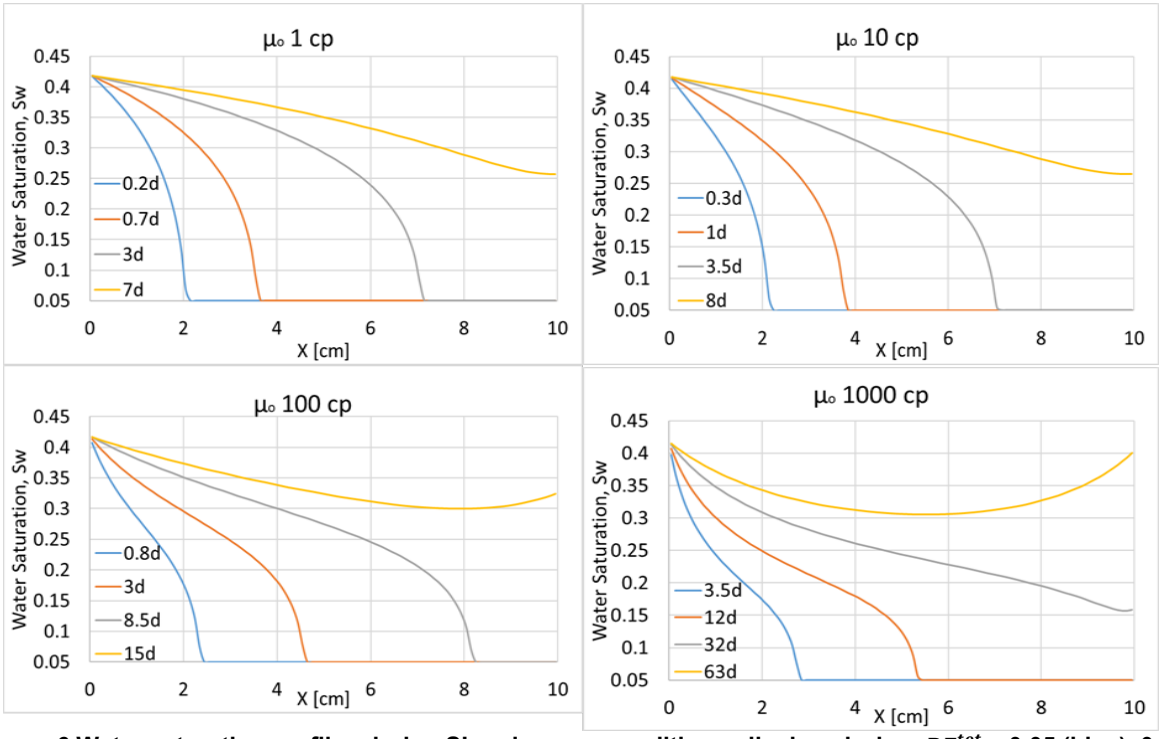

Figure 6 Water saturation profiles during SI under *pww* conditions, displayed when RF^{tot} = 0.05 (blue), 0.10 (orange), 0.20 (grey) and 0.30 (yellow) for different oil viscosities. The absolute times are indicated.

Several authors (Li et al. 2006; Unsal et al. 2007; Haugen et al. 2014; Fernø et al. 2015; Andersen et al. 2019a,b) have pointed out the importance of the capillary back pressure during co-current SI, especially as a limitation for counter-current production. Those and other studies have as far as we know, focused on SWW media.

We have seen from the presented cases on MW media that counter-current production makes a strong contribution and we therefore expect the capillary back pressure to play an important role. We show RF^{tot} (solid lines) and RF^{cou} (dashed lines) for *pow* (**Figure 7**) and *pww* (**Figure 8**) cases at two oil viscosities; 1 cP (base) and 100 cP. For each of these four variations the capillary back pressure (to oil at the inlet) P_{cbo} is varied from 0 to 0.1 to 0.5 bar. For the low oil viscosity case (1 cP) the counter-current production is very sensitive to P_{cbo} and rapidly falls to negligible amounts (less than 1 tenth of the total production) already at a value of 0.1 bar, for both the *pow* and *pww* cases. The counter-current production is practically eliminated at P_{cbo}= 0.5 bar. The total recovery curves are barely affected by this change, indicating that the same amount of water imbibes at the inlet, while the oil production shifts towards the outlet side. For the high oil viscosity case (100 cP), the increase of P_{cbo} to 0.1 bar reduces the counter-current production by roughly one fifth and increasing it to 0.5 bar reduces it by four fifths of the original level for both *pow* and *pww* states. The total recovery factor is delayed correspondingly, but approaches the same ultimate recovery given sufficient time.

Increasing P_{cbo} forces more oil to be produced towards the outlet by flowing through the initially oil-saturated region. When this region has low mobility it takes more time for the capillary forces to displace the same amount of oil from the system compared to when some of the oil could flow out at the inlet through the high mobility zone. When that region has high mobility, it makes little difference if all the oil must leave that direction. The sensitivity of the low viscosity cases to the back pressure can be attributed to the mobility ratio and saturation profiles, see **Figure 5** and **Figure 6**. At favorable mobility ratio the saturation profiles are steeper and less dominated by intermediate saturations. The high saturations corresponding to low capillary pressure create a low driving force for oil to flow towards the inlet, but are helped by the high mobility. Once the inlet back pressure is increased the pressure difference is quickly

eliminated. At unfavorable mobility, there are more intermediate saturations with high capillary pressure and a greater driving force less affected by the same level of P_{cbo}.

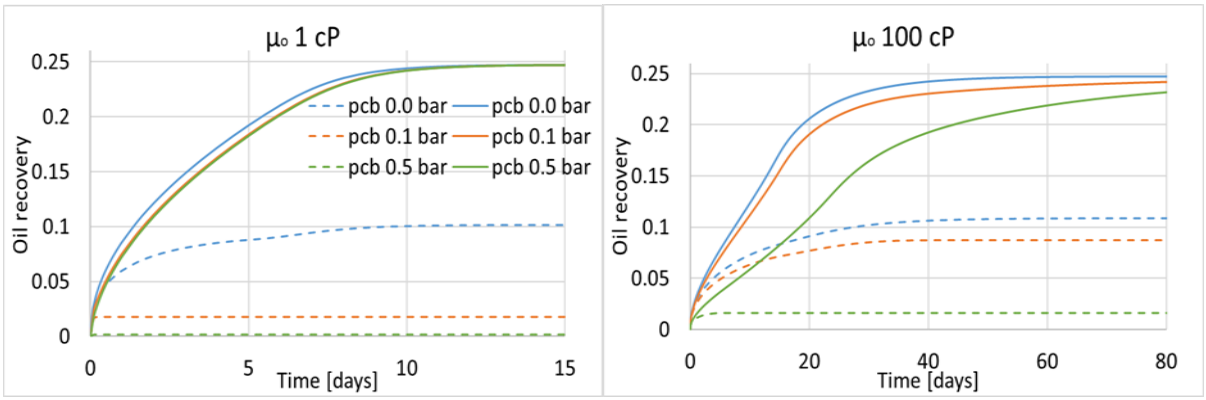

Figure 7 The effect of capillary back pressure on SI at fixed *pow* wetting state. The solid lines indicate total recovery, while the dashed lines indicate counter-current recovery.

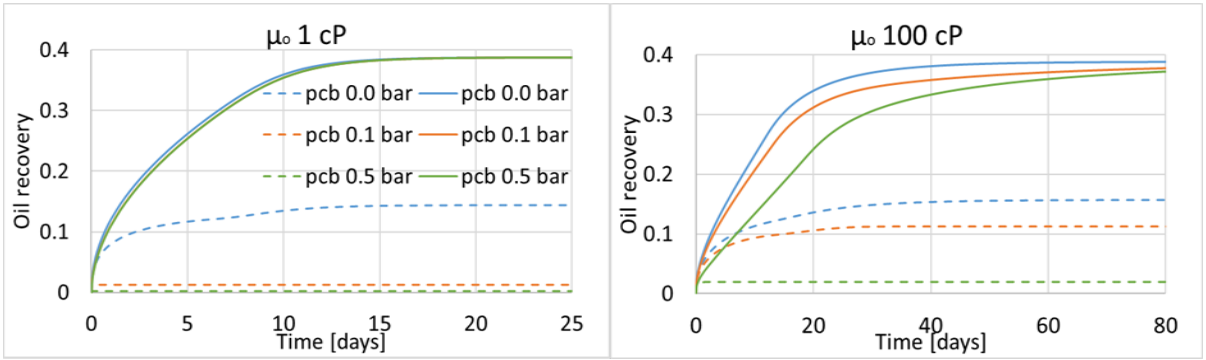

Figure 8 The effect of capillary back pressure on SI at fixed *pww* wetting state. The solid lines indicate total recovery, while the dashed lines indicate counter-current recovery.

3.3. Secondary imbibition enhanced recovery

In this section we explore co-current SI when the imbibing brine contains WA component from the start. This would correspond to a situation where the first injected water in a field is not in equilibrium with the formation.

First we consider the role of varying the WA component concentration in the imbibing brine from 0 to 1 in intervals of 0.25. The initial state is *pow*. If $c = 0$ the wetting remains *pow* and if $c = 1$ it will eventually become *pww*, while for intermediate concentrations; somewhere in between. This is tested for the case with oil viscosity of 1 cP (left) and 100 cP (right) where RF^{co} and RF^{cou} are shown vs time for different concentrations in **Figure 9**. Water saturation $s_w(x)$ and WA component concentration $c(x)$ distributions after 10 d are shown in **Figure 10**.

For both low and high oil viscosity cases it is seen in **Figure 9** that counter-current recovery RF^{cou} is affected by WA component from the start. This is natural since capillary pressure is raised locally, the water pressure becomes more negative and the oil pressure becomes more positive near the inlet. Since the inlet has both phase pressures equal zero (according to boundary condition $P_c = 0$) the fluxes of both phases increase in magnitude, and in opposite direction. Further, oil mobility in the WA affected region is improved by increased oil relative permeability. On the other hand, the impact on RF^{co} is not seen until late times. The intermediate time co-current recovery appears to stabilize at somewhat lower values (~0.01) when WA takes place indicating that the WA near the inlet diverts more oil to flow out the inlet than the outlet. This stabilization indicates that the system is limited by the diffusive transport of WA component which has larger time scale. Significant differences are seen mainly after recovery for the *pow* case $(c = 0)$ has stabilized (ca 10 d for 1 cP and 40 d for 100 cP) when

the elevated capillary forces from WA also increase co-current production. Ultimately the levels of RF^{cou} become very similar to those of RF^{co}: namely 0.18 vs 0.205 for 1 cP and 0.20 vs 0.18 for 100 cP considering the $c = 1$ case. I.e., the counter-current recovery can dominate the co-current recovery. Comparing to **Figure 4** we see that a system starting out as *pww* had significantly higher co-current production than counter-current production. In other words, the WA process seems to boost counter-current production more than co-current production.

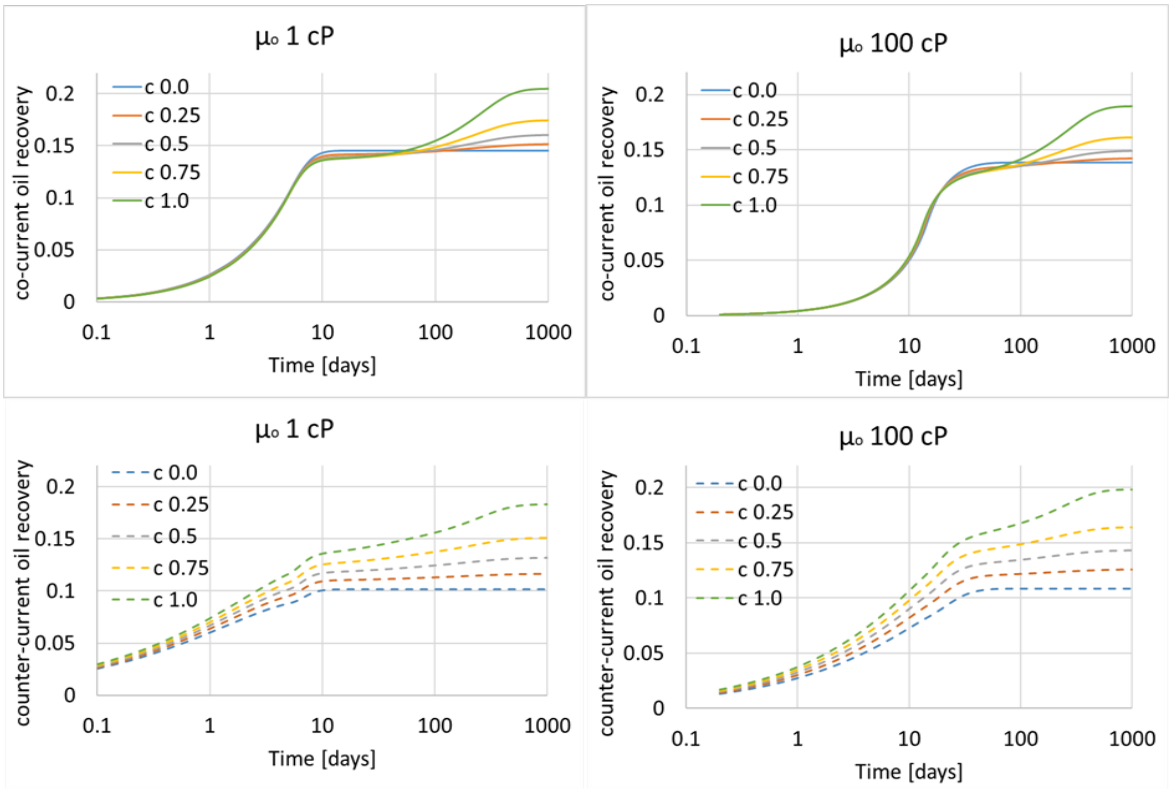

Figure 9 Secondary imbibition enhanced oil recovery where brine with WA component imbibes from initial time for different concentrations. The left figures indicate cases with oil viscosity of 1 cP, while right figures indicate cases with 100 cP oil viscosity. $P_{cbo} = 0$ was assumed. Co-current recovery RF^{co} (solid lines) and counter-current recovery RF^{cou} (dashed lines) are displayed in row 1 and 2, respectively.

In **Figure 10** it is seen that after 10 d the saturations have reached $s_{w,eq}^{pow} = 0.284$ across the core for the 1 cP case, in line with **Figure 9** where recovery has stabilized at that time for the *pow* case. The cases where a nonzero concentration has imbibed display a concentration front that has travelled roughly half way into the core with the highest concentrations at the inlet and zero concentrations centrally and towards the outlet. Especially, the concentrations have travelled shorter distance than the brine which has travelled through the entire core to the outlet. The delay of the concentration is partly due to dilution in the connate water, but primarily due to adsorption; with $k_d = 1$ the flux of concentration is roughly half that of the water. Diffusion acts very slowly and does not efficiently spread the component at this early stage of the process, but becomes more effective as the saturations increase, see (6). As the saturations cannot increase beyond the concentration dependent $s_{w,eq}$ the saturation profiles only differ near the inlet for the 1 cP case at that specific time. For the 100 cP case it is seen that the concentrations have not reached more than half the core after 10 d, but impact the entire saturation profiles which extend over 80 % of the core by showing increased water content. The WA component raises the capillary forces and thus affects the phase pressure profiles which run continuously throughout the core. Resultingly, the impact of WA can be seen far from where the component has reached. Note however, that most of the added production at this time (10 d) is counter-

current as shown in **Figure 9**, while no significant addition to co-current production is seen until after 100 d.

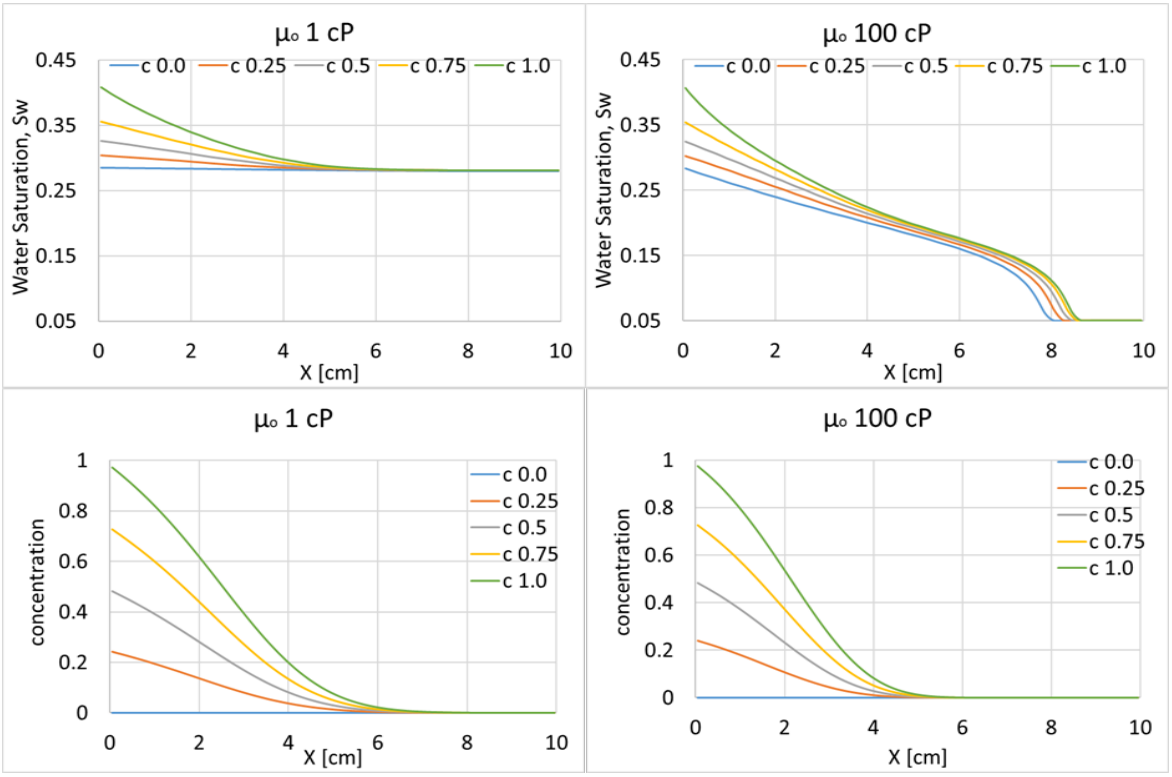

Figure 10 Secondary imbibition enhanced oil recovery where brine with WA component imbibes from initial time for different concentrations. The left figures indicate cases with oil viscosity of 1 cP, while right figures indicate cases with 100 cP oil viscosity. $P_{cbo} = 0$ was assumed. Water saturation profiles and concentration profiles after 10 d are shown in row 1 and row 2, respectively.

In **Figure 11** we show the same case as in **Figure 9** and **Figure 10**, except that a high capillary back pressure of $P_{cbo} = 1$ bar has been used, instead of 0 bar. This effectively eliminates the counter-current production, hence only the co-current production (effectively the total production) is shown in row 1, for the case with 1 cP oil (left) and 100 cP oil (right). The behavior in this case seems to combine elements of the previous; although the recovery is concentration dependent from the start, the differences are mainly significant at late times, approximately when recovery in the *pow* case seems to stabilize (10 d for 1 cP and 100 d for the 100 cP case). Capillary SI of brine with WA component increases the capillary forces and therefore also the imbibition rate. However, the component is adsorbed and diluted into the connate water and so the process slows down when the capacity to advect brine with component into the system is met. That is roughly after 10 d for the 1 cP system. The full potential is limited by diffusion transport which is a slow process and seems to have a time scale of 500 d for both 1 and 100 cP cases. As the 100 cP case has a slower capillary imbibition process initially the transition into the diffusion dominated domain is more gradual. For nonzero concentrations; whether the oil viscosity is high or low or the back pressure is zero or high, the recovery process seems to terminate after roughly 1000 d. This is two orders of magnitude greater time than the *pow* case with 1 cP oil (10 d) and one order greater than the *pow* case with 100 cP oil (100 d). This further indicates that diffusion is the limiting mechanism of WA at late times. At early times the saturation and concentration profiles show great influence from both viscosity and back pressure. Especially, for a given back pressure; a high oil viscosity leads to less imbibed water and WA component after 10 days compared to low oil viscosity (compare left and right plots in **Figure 10** and **Figure 11**). Further, for a given oil viscosity, increasing the back

pressure reduces the amount of water and WA component imbibed after 10 d (compare row 1 and 2 in **Figure 10** with row 2 and 3 in **Figure 11**).

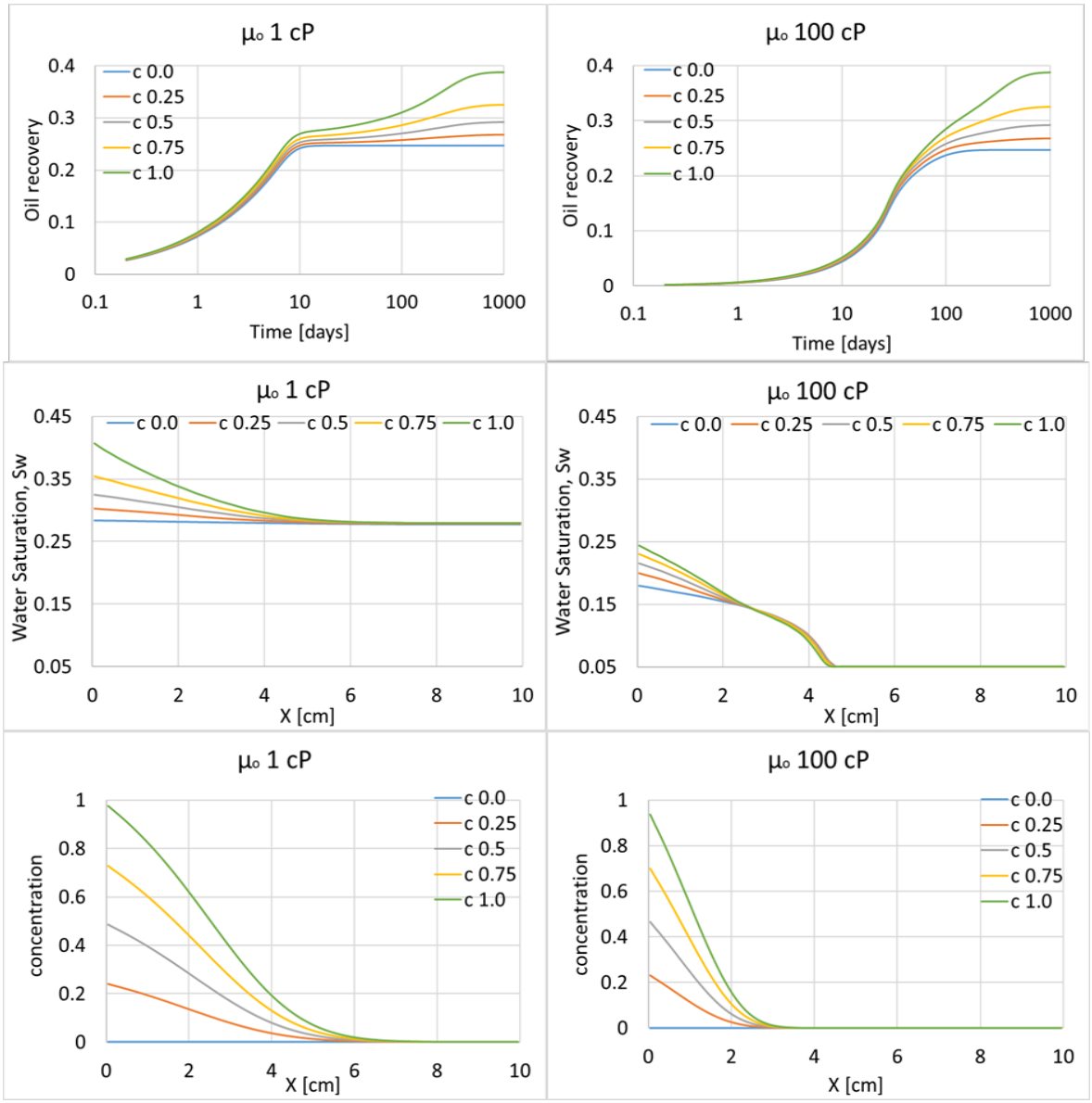

Figure 11 Secondary imbibition enhanced oil recovery where brine with WA component imbibes from initial time for different concentrations. The left figures indicate cases with oil viscosity of 1 cP, while right figures indicate cases with 100 cP oil viscosity. A capillary back pressure of 1 bar was assumed to eliminate counter-current production. $RF^{co} = RF^{tot}$ is displayed in row 1. Water saturation profiles and concentration profiles after 10 d are shown in row 2 and row 3, respectively.

The role of the distribution coefficient k_d is evaluated in the next example. This parameter states how much WA component is adsorbed compared to the amount of component in the brine. The co-current recovery and counter-current recovery vs time are plotted in **Figure 12** in row 1 and 2, respectively. A concentration $c = 1$ was applied, the oil viscosity was either 1 cP (left) or 100 cP (right) and P_{cbo} was 0 bar. The same case with back pressure $P_{cbo} = 1$ bar is shown in row 3 of **Figure 12**, where only total recovery is shown since the counter-current production is zero.

Primarily, increased adsorption causes a delay in how quickly the WA component can travel through the core and thus delays recovery. The behavior is then similar to that of *pow* state for longer time. Especially, for large k_d more of the WA component that is transported

into the core carried by the imbibing brine is adsorbed. Hence, it is primarily diffusion that facilitates WA for such cases. For the cases with $P_{cbo} = 0$ bar we see that increased k_d leads to accelerated co-current production when the time scale reflects that of the diffusion. Counter-current SI is affected by WA component from the start, although high k_d reduces the impact. Interestingly, an important, but opposite trend seems to be that the amount of co-current production increases when adsorption increases, while the counter-current production decreases correspondingly. This occurred both for high and low oil viscosity cases although a higher level of counter-current production was observed for high oil viscosity.

At a high back pressure (row 3), all the production is co-current. The recovery curves look similar at early times, and reflect that the WA process occurs slowly compared to the imbibition rate initially. Significant initiation of WA seems to occur at different times for the two viscosity cases, but diffusion being the controlling factor, the processes stabilize at very similar times for equal values of k_d despite different viscosities.

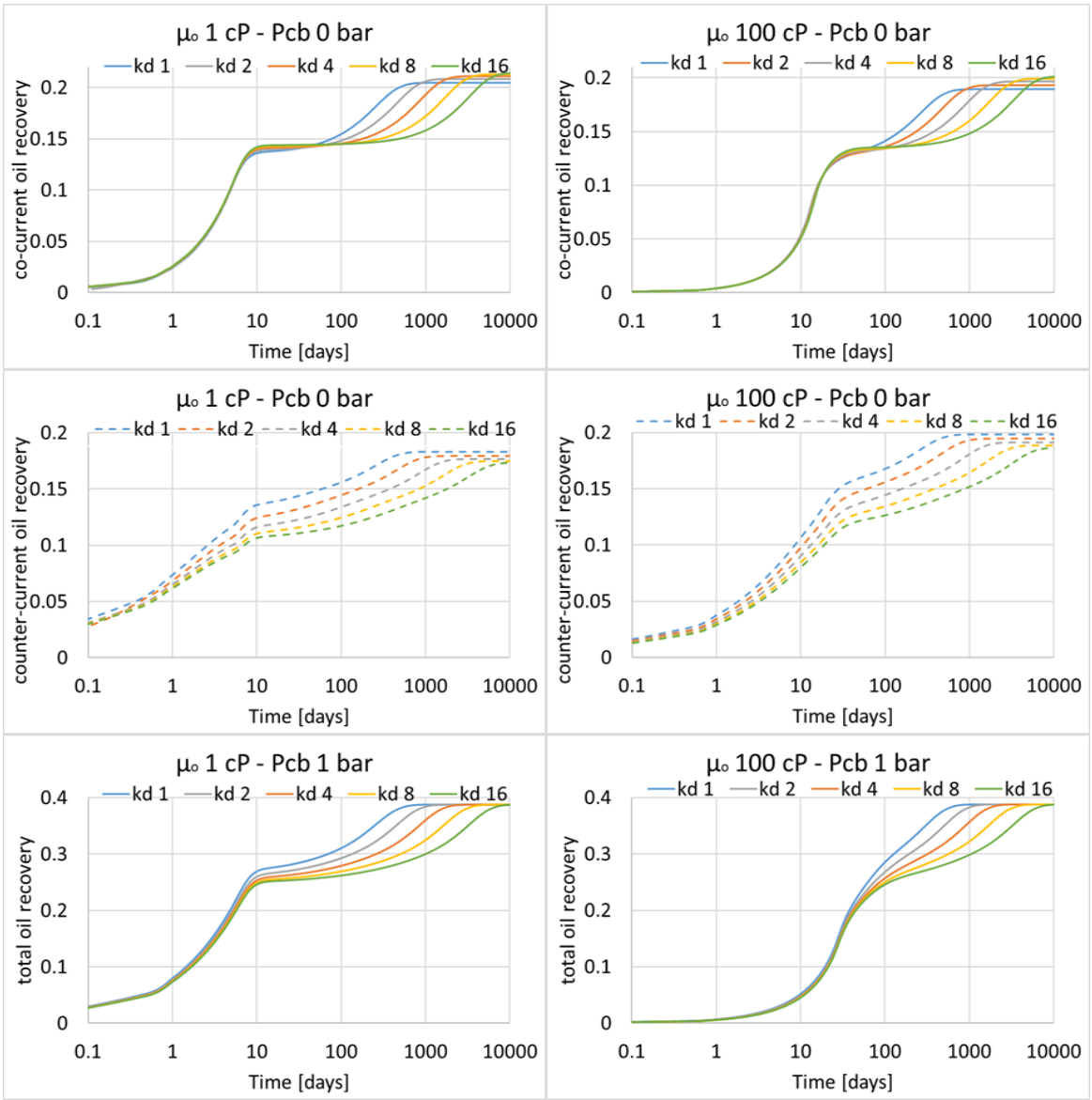

Figure 12 The role of adsorption distribution coefficient k_d on imbibition behavior for oil viscosity of 1 cP (left) and 100 cP (right) when WA with $c = 1$ is performed. RF^{co} and RF^{cou} are shown in row 1 and 2, respectively, for the case of a zero capillary back pressure. In row 3 a back pressure of 1 bar is assumed and $RF^{co} = RF^{tot}$ is shown (no counter-current production).

3.4. Tertiary imbibition enhanced recovery

In this section we consider tertiary EOR by WA in the sense that the imbibing brine initially does not contain WA component, but WA component is added to the imbibing brine with concentration $c = 1$ after a specified time, where a significant recovery has been obtained. For 1 cP viscosity oil these times are 0, 2, 4, 8 or 16 d while for 100 cP viscosity oil the times are 0, 4, 8, 16 or 32 d. They are compared to the pow case where no WA takes place. At 0 d no SI of inert brine has occurred, while at the last specified time (16 or 32 d), almost all SI corresponding to the *pow* state has occurred. This means that no initial capillary forces remain to transport WA component into the core and this must be done entirely by diffusion. The results are presented in **Figure 13**. The co-current and counter-current recovery profiles vs time are shown in row 1 and 2, respectively.

As before, co-current recovery is not greatly affected by WA at early times. Almost regardless of when the imbibed brine is spiked with WA component the co-current recovery profiles look practically identical with no clear events indicating the WA process having started. Particularly they overlap closely with the curve corresponding to fixed *pow* state until the capillary forces of that state are vanished. At late times, (ca 30 d for both viscosity cases) the profiles begin to accelerate due to diffusion becoming important. A main distinction is the case where WA component was used in the imbibing brine from the start showing lower end co-current recovery than the remaining cases. The end level appears to increase with spiking the brine later for the 100 cP case, while the distinction is not clear for the 1 cP case. The impact on counter-current recovery is much clearer and this production accelerates almost immediately when the WA component is introduced. The end levels tend to increase if the component is introduced at earlier times, most clearly seen for the 100 cP case. The results indicate that although WA improves both co- and counter-current recovery, it initially may divert oil towards the inlet and primarily boosts counter-current production. Mainly at late times, when diffusion has increased capillary forces throughout the system does the WA lead to enhanced co-current recovery.

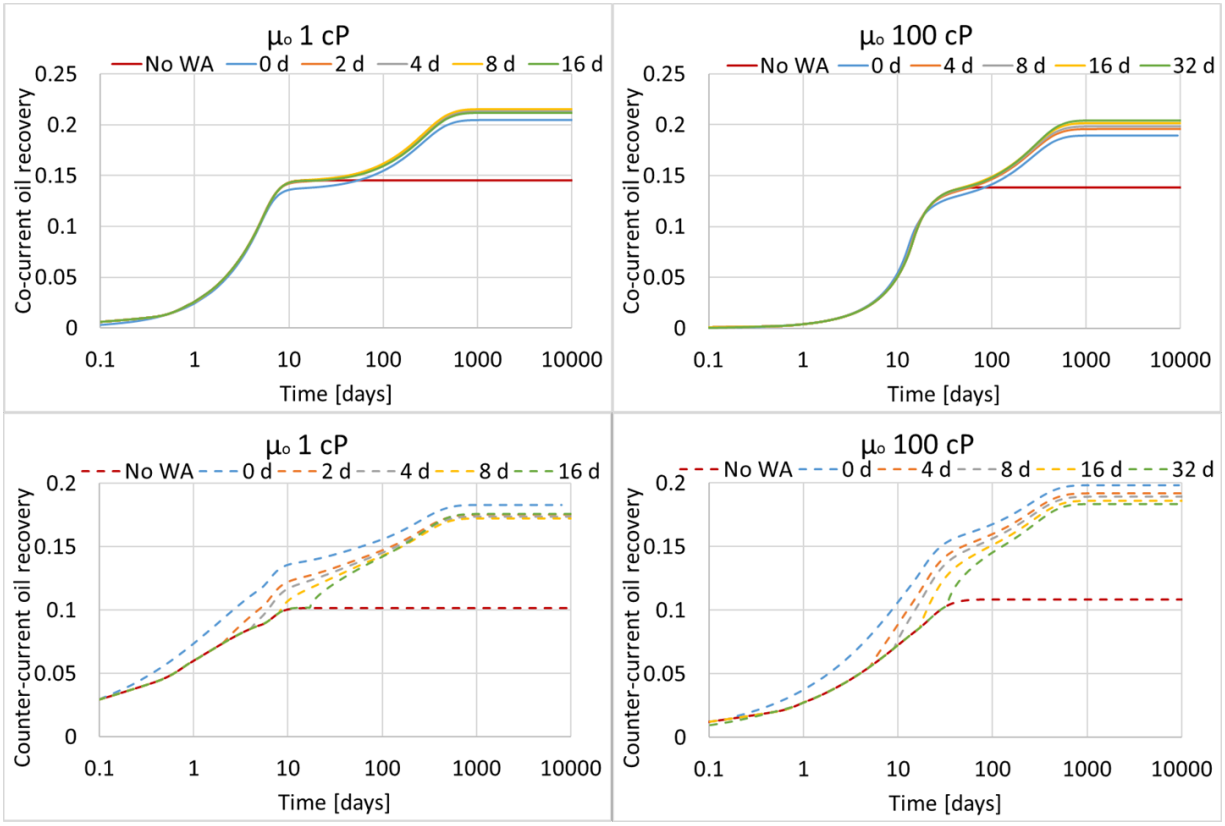

Figure 13 Tertiary oil recovery for oil viscosity 1 cP (left) and 100 cP (right). Initially water imbibes with $c = 0$ such that pow state remains for some time. At the indicated times brine with concentration $c = 1$ imbibes. RF^{co} and RF^{cou} are shown in row 1 and row 2, respectively. Zero capillary back pressure is assumed.

The example was repeated when a high capillary back pressure of 1 bar was used at the inlet (no counter-current oil production). The co-current (total) recovery vs time is shown in **Figure 14**. Interestingly, although the WA component is introduced at very different times in terms of how much of the initial capillary forces are present or left, there is very little distinction between the profiles. Hence, the main contributor to the WA process is the diffusion and the amount brought in by initial capillary forces does not appear to play an important role.

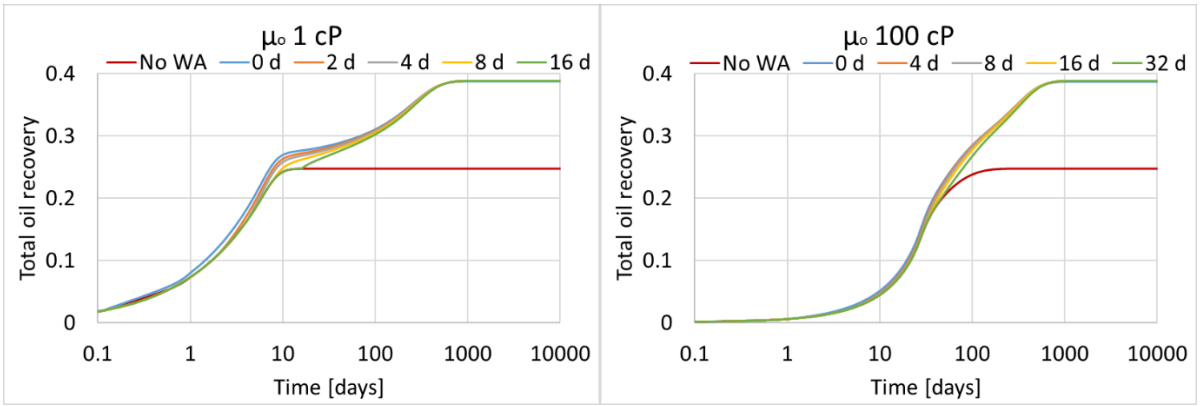

Figure 14 Tertiary oil recovery for oil viscosity 1 cP (left) and 100 cP (right). A capillary back pressure of 1 bar is assumed to eliminate counter-current production. Initially water imbibes with $c = 0$ such that pow state remains for some time. At the indicated times brine with concentration $c = 1$ imbibes. $RF^{co} = RF^{tot}$ is shown.

3.5. Controls on counter-current production

In this section we investigate what controls the level of counter-current production. The initial oil mobility $\lambda_o(s_{wi})$ ahead of the water front determines how easily oil can be displaced towards

the outlet. In comparison, a characteristic mobility for counter-current SI is given by $\frac{\lambda_o\lambda_w}{\lambda_o+\lambda_w} = \frac{1}{1/\lambda_o+1/\lambda_w}$ (see for example Zhou et al. (2002) and Standnes and Andersen (2017)), which we here evaluate at the intermediate representative saturation $\hat{s}_w = \frac{s_{wi}+s_{w,eq}}{2}$. If the former mobility is large compared to the latter, we expect a dominance of co-current production, and if opposite, we expect significant counter-current production. Hence, the following mobility ratio M^* is introduced:

$$M^* = \frac{\lambda_o(s_{wi})}{\frac{1}{1/\lambda_o(\hat{s}_w) + 1/\lambda_w(\hat{s}_w)}}, \tag{28}$$

For large oil mobility, M^* is high and simplified to:

$$M^* \approx M^*_{\lambda_o+} = \frac{\lambda_o(s_{wi})}{\lambda_w(\hat{s}_w)} \gg 1, \qquad (\text{low } RF^{cou}) \tag{29}$$

while for small oil mobility M^* is low and simplified to:

$$M^* \approx M^*_{\lambda_o-} = \frac{\lambda_o(s_{wi})}{\lambda_o(\hat{s}_w)} = \frac{k_{ro}(s_{wi})}{k_{ro}(\hat{s}_w)} > 1, \qquad (\text{high } RF^{cou}) \tag{30}$$

If the oil mobility becomes infinite, so does M^* (and $M^*_{\lambda_o+}$) which should correspond to low counter-current production. Experimentally it is also seen that high mobility of non-wetting phase compared to wetting phase gives low counter-current (Haugen et al. 2014; Hamidpour et al. 2015; Meng et al. 2016, 2017; Andersen et al. 2019a). The comparatively low wetting phase mobility can also be a result of the wettability, i.e. the wetting phase tends to have low relative permeability (Anderson 1987b; McPhee et al. 2015). On the other hand, for low oil mobility, M^* (and hence $M^*_{\lambda_o-}$) becomes independent of both phase viscosities and $M^*_{\lambda_o-}$ denotes a lower bound. If the medium is less water-wet, $\hat{s}_w$ is lower, increasing the mobility of the oil in the twophase region, and the bound $M^*_{\lambda_o-}$ is increased (assuming same relative permeability functions). This behavior may suggest that at sufficiently high oil viscosity, the fraction of counter-current production reaches an upper limit that is independent of oil viscosity; and that the fraction increases if the medium is less water-wet.

We consider all four combinations of relative permeabilities $\left(k_{ri}^{pow}, k_{ri}^{pww}\right)$ and capillary pressure curves (J^{pow}, J^{pww}) (the former rescaled to the saturation interval of the J-functions). That allows to see the effect of only changing relative permeability vs only changing the J-function. The mobility ratios M^* for these function combinations are calculated for non-wetting phase viscosity varied from 0.001 cP (similar to air) up to 10 000 000 cP (similar to bitumen), i.e. 10 orders of magnitude, and corresponding SI simulations are run for every viscosity separated by a factor of 10 in that range. The fraction of counter-current production (RF^{cou}/RF^{tot}) after completed SI is plotted against viscosity in **Figure 15** left and against M^* in **Figure 15** right.

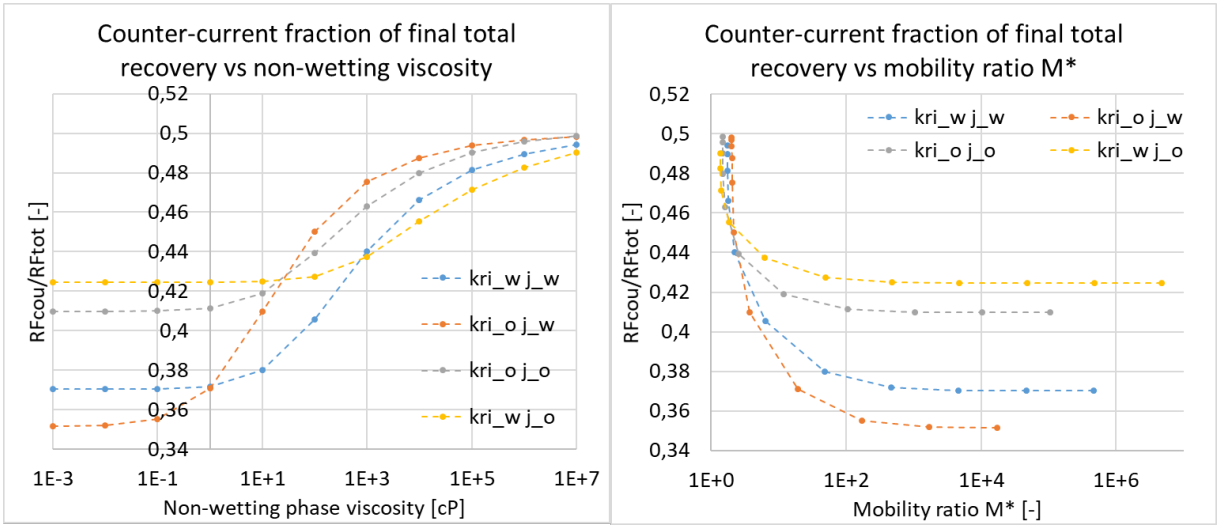

Figure 15 The fraction of counter-current production out of total production at end of SI plotted against viscosity (left) and mobility ratio M^* (right). The combinations of saturation functions are indicated. Results from simulations are shown as points, while the lines are intended to indicate trends.

As expected, reduced viscosity, i.e. larger M^* leads to lower fraction of counter-current production. For each of the four cases a stable fraction is obtained at high and low viscosities that is insensitive to further viscosity changes. The low fraction level is in all cases entered at $M^* \approx 1000$, which appears to be a critical value. Comparatively, three orders of magnitude separate the viscosities where the level is reached. On the opposite side of the scale, when $M^* \approx 3$ the highest amount of counter-current production is achieved, which for all cases appears to be 0.5, in other words just as much oil can be produced from the inlet as from the outlet under very high oil viscosity conditions. As this fraction was approached irrespective of the combination of saturation functions it appears to be a general result. Note also that 8 orders of magnitude variation of viscosity appears to be the range required to go from the lowest to the highest fraction of counter-current production.

The lowest fraction of counter-current production is 0.35 which is very high compared to what is reported for SWW cases (5-10 %) at typical conditions, although much higher fractions were reported at unfavorable mobility ratio by Haugen et al. (2015) and Meng et al. (2017). The likely cause of this is the use of mixed-wet saturation functions which assert a saturation range in the lower range where oil has high mobility in the multiphase region: For the same set of relative permeabilities, using the pow J-function significantly increases the counter-current fraction: for k_{ri}^{pow} the lowest fraction increases from 0.35 to 0.41 while for k_{ri}^{pww} it increases from 0.37 to 0.425. As we see, however, both types of saturation functions determine the amount of counter-current production as each combination of functions obtains a different level at high M^*.

We next look more closely at how the distribution of co-current and counter-current oil production is affected by wettability alteration. We assume that wettability is altered towards water-wet by shifting J^{pow} to J^{pww}, but consider four combinations of shifting relative permeabilities: k_{ri}^{pow} to k_{ri}^{pww}, k_{ri}^{pww} to k_{ri}^{pow}, k_{ri}^{pww} to k_{ri}^{pww} (no shift), k_{ri}^{pow} to k_{ri}^{pow} (no shift). This is repeated for viscosities ranging from 0.01 cP to 10 000 cP every factor 10. The ratio of counter-current fraction with WA, $\left(\frac{RF^{cou}}{RF^{tot}}\right)^{WA}$, divided by the fraction without WA, $\left(\frac{RF^{cou}}{RF^{tot}}\right)^{ref}$ is plotted against viscosity in **Figure 16**. The reference is based on saturation functions identical to those of the original state during the corresponding WA case.

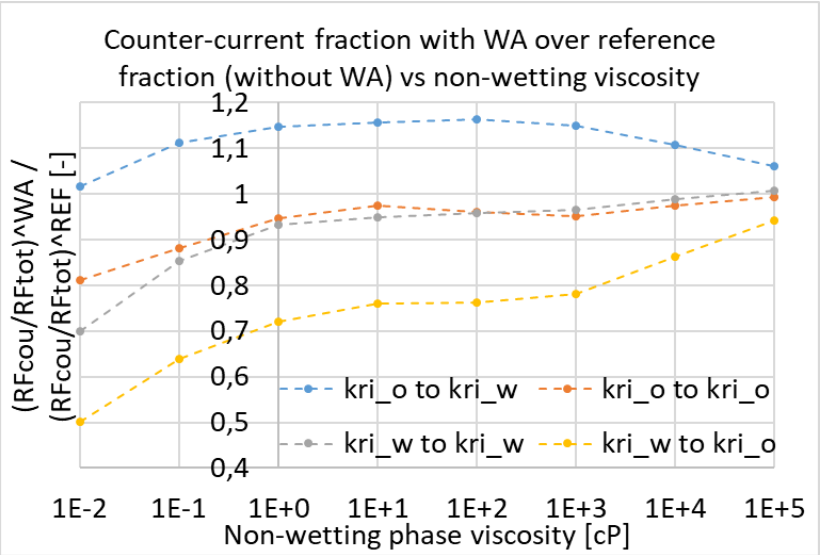

Figure 16 The ratio $\left(\frac{RF^{cou}}{RF^{tot}}\right)^{WA} / \left(\frac{RF^{cou}}{RF^{tot}}\right)^{ref}$ plotted against viscosity for different shifts in relative permeability during WA.

We see that WA changes the distribution of counter-current vs co-current recovery. When the same relative permeabilities are used, and only the J-function is shifted by WA, the distribution is close to the same as without WA (the ratio is ca 0.95) except for at low viscosities (~0.01 cP) where it is reduced to 0.7-0.8 of the fraction without WA, i.e. the WA then adds more recovery to co-current production than counter-current. For the case where the k_{ri}^{pww} set is shifted to the k_{ri}^{pow} set, the counter-current ratio is significantly reduced compared to the reference indicating that most of the added recovery is gained co-currently. We note that the k_{ri}^{pww} set has high oil mobility compared to the k_{ri}^{pow} and this shift from the former to the latter set may have induced an effective oil blockage near the inlet, while the raised capillary forces have contributed to push the oil towards the outlet instead. Similarly, when the k_{ri}^{pow} set is shifted to k_{ri}^{pww} the oil is given more mobility at the inlet thus boosting counter-current production compared to co-current production, and increasing the fraction by as much as 15% compared to the reference. The latter is assumed to be representative when wettability shifts towards more water-wet.

3.6. Model limitations

We have assumed a smart water type of WA agent acting primarily on the saturation functions. Surfactants or other chemicals might affect interfacial tension, bulk fluid properties such as viscosity and density or residual saturations more directly (Delshad et al. 2009). More comprehensive chemical modeling might better capture the reactive brine-rock-oil interplay driving WA. Here this has been simplified to an adsorption type process of a single transported component. The WA can also be handled using a different interpolation between the saturation functions than linearly (with adsorption), or linking the interpolation to other parameters such as surface complexation (Qiao et al. 2014).

4. Conclusions

A simulation study has been presented on co-current spontaneous imbibition (SI) in mixed-wet (MW) media subject to wettability alteration (WA) from a preferentially oil-wet system towards more water-wet by the adsorption of a general WA component. The following conclusions are drawn from this work:

- Co-current SI in MW systems shows:

    - Steady imbibition towards zero capillary pressure even for highly unfavorable mobility ratios. This is contrary to SWW systems where imbibition rate falls drastically at low recovery factors in systems with unfavorable mobility ratio. The oil does not obtain severe mobility reduction in MW systems when water reaches the outlet side since the oil saturation does not approach its critical value as it may in SWW systems.
    - High fraction of counter-current production (more than a third) was observed for MW cases explained by the high oil mobility at the inlet compared to SWW systems. Variation of viscosity by 10 orders of magnitude and systematic variation of relative permeability and capillary pressure demonstrated that a lower bound of counter-current production exists for given saturation functions. If oil viscosity is increased sufficiently, half the production is counter-current.
    - the high counter-current production is sensitive to the capillary back pressure, especially for high mobility of the non-wetting phase compared to the wetting phase. For such cases the total production was however, barely affected by the back pressure. For cases where the non-wetting phase was less sensitive to the back pressure, a reduction of the counter-current production by increased back pressure led to delayed total production.
- In the case of WA from a preferentially oil-wet towards a preferentially water-wet system it was observed that:
    - Introducing WA component at the inlet immediately accelerated the counter-current production, but did not impact the co-current production until very late times, at which also this would increase.
    - The added recovery by WA was significant on both sides of the core, but in our examples twice as much of the incremental recovery was at the inlet side (counter-current) as at the outlet side (co-current). Systematic analyses showed that the increase of oil mobility in the WA affected inlet region explained the preferential increase of counter-current imbibition and that curves shifted towards lower oil mobility would reduce counter-current production.
    - Diffusion seems to be a limiting mechanism for co-current imbibition EOR. The WA component brought in by imbibing brine is diluted and adsorbed and diffusion is required to affect the process effectively at the front. For this reason, adsorption directly delayed the recovery process at late times.
    - The point in time at which WA component was introduced during the process did not have much impact on the co-current recovery profiles which overlapped closely at all times. The counter-current recovery profiles were however accelerated and also their end levels became slightly higher if WA component was introduced earlier, with an opposite impact on the co-current end recovery. The difference was greater for low non-wetting phase mobility.
    - When a high capillary back pressure was used, all the production, including that from WA was produced co-currently at the outlet. This was strongly limited by diffusion which seemed to reduce the importance of other parameters such as the time of component exposure.

We emphasize that many of these trends are predictions from a simulation study (parameterized based on realistic input data), but there are few experimental results in the literature to compare with. Particularly, we encourage more systematic experimental investigations of co-current SI to be performed with non-zero initial saturation; mixed-wet conditions; and wettability alteration.

Acknowledgments

The authors acknowledge the Research Council of Norway and the industry partners, ConocoPhillips Skandinavia AS, Aker BP ASA, Eni Norge AS, Equinor ASA, Neptune Energy Norge AS, Lundin Norway AS, Halliburton AS, Schlumberger Norge AS, Wintershall Norge AS, and DEA Norge AS, The National IOR Centre of Norway for support. We thank Arild Lohne (NORCE) for providing IORCoreSim support.

References

1. Ahsan, R., Madland, M. V., Bratteli, F., & Hiorth, A. (2012, August). A Study of Sulphate Ions-Effects on Aging and Imbibition Capillary Pressure Curve. In *International Symposium of the Society of Core Analysts*.
2. Akin, S., Schembre, J. M., Bhat, S. K., & Kovscek, A. R. (2000). Spontaneous imbibition characteristics of diatomite. *Journal of Petroleum Science and Engineering*, *25*(3-4), 149-165.
3. Andersen, P. Ø., Evje, S., Kleppe, H., & Skjæveland, S. M. (2015). A model for wettability alteration in fractured reservoirs. *SPE Journal*, **20**(06), 1-261.
4. Andersen, P. Ø., Skjæveland, S. M., & Standnes, D. C. (2017a). A Novel Bounded Capillary Pressure Correlation with Application to Both Mixed and Strongly Wetted Porous Media. In *SPE Abu Dhabi International Petroleum Exhibition & Conference, Abu Dhabi, UAE*.
5. Andersen, P. Ø., Evje, S., & Hiorth, A. (2017b). Modeling of Spontaneous-Imbibition Experiments With Porous Disk—On the Validity of Exponential Prediction. *SPE Journal*, **22**(05), 1-326.
6. Andersen, P. Ø., Brattekås, B., Nødland, O., Lohne, A., Føyen, T. L., & Fernø, M. A. (2019a). Darcy-Scale Simulation of Boundary-Condition Effects During Capillary-Dominated Flow in High-Permeability Systems. *SPE Reservoir Evaluation & Engineering,* **22**(02), 673-691.
7. Andersen, P. Ø., Qiao, Y., Standnes, D. C., & Evje, S. (2019b). Cocurrent spontaneous imbibition in porous media with the dynamics of viscous coupling and capillary backpressure. *SPE Journal*, **24**(01), 158-177.
8. Andersen, P. Ø. (2019). A simplified modelling approach for petroleum recovery by spontaneous imbibition in naturally fractured reservoirs. *Journal of Natural Gas Science and Engineering*, **63**, 95-114.
9. Andersen, Ø. P. (2020a). Early and Late Time Analytical Solutions for Co-Current Spontaneous Imbibition and Generalized Scaling. In *SPE Europec featured at 82nd EAGE Conference and Exhibition*.
10. Andersen (2020b). Capillary Pressure Effects on Estimating the Enhanced-Oil-Recovery Potential During Low-Salinity and Smart Waterflooding. *SPE Journal*.
11. Anderson, W. G. (1987a). Wettability literature survey-part 4: Effects of wettability on capillary pressure. *Journal of petroleum technology*, *39*(10), 1-283.
12. Anderson, W. G. (1987b). Wettability literature survey part 5: the effects of wettability on relative permeability. *Journal of Petroleum Technology*, *39*(11), 1-453.
13. Appelo, C. A. J., & Postma, D. (2005). Geochemistry, groundwater and pollution. 2nd. *Ed. Balkema, Rotterdam*.
14. Aronofsky, J. S., Masse, L., & Natanson, S. G. (1958). A model for the mechanism of oil recovery from the porous matrix due to water invasion in fractured reservoirs. *Petroleum Transactions, AIME*, **213**, 17-19.
15. Babadagli, T. (2000). Scaling of Co-Current and Counter-Current Capillary Imbibition for Surfactant and Polymer Injection in Naturally Fractured Reservoirs. In SPE/AAPG Western regional meeting, Long Beach, California, 19-23 June.
16. Babadagli, T. (2005). Analysis of oil recovery by spontaneous imbibition of surfactant solution. *Oil & gas science and technology*, *60*(4), 697-710.

17. Behbahani, H., & Blunt, M. J. (2005). Analysis of imbibition in mixed-wet rocks using pore-scale modeling. *Spe Journal*, *10*(04), 466-474.
18. Bourbiaux, B. J., & Kalaydjian, F. J. (1990). Experimental study of cocurrent and countercurrent flows in natural porous media. *SPE Reservoir Engineering*, *5*(03), 361-368.
19. Brooks, R. H., & Corey, A. T. (1966). Properties of porous media affecting fluid flow. *Journal of the Irrigation and Drainage Division*, **92**(2), 61-90.
20. Buckley, S. E., & Leverett, M. (1942). Mechanism of fluid displacement in sands. *Transactions of the AIME*, **146**(01), 107-116.
21. Chen, Z., Huan, G., & Ma, Y. (2006). *Computational methods for multiphase flows in porous media* (Vol. 2). SIAM.
22. Dang, C. T. Q., Nghiem, L. X., Chen, Z. J., & Nguyen, Q. P. (2013, September). Modeling low salinity waterflooding: ion exchange, geochemistry and wettability alteration. In *SPE Annual Technical Conference and Exhibition*.
23. Delshad, M., Najafabadi, N. F., Andersen, G. A. et al. 2009. Modeling wettability alteration by surfactants in naturally fractured reservoirs. *SPE Reservoir Evaluation and Engineering 12*, 361-370.
24. Fernø, M. A., Haugen, Å., Brattekås, B., Morrow, N. R. and Mason, G. (2015). Spontaneous Imbibition Revisited: A New Method to Determine Kr and Pc by Inclusion of the Capillary Backpressure. In *The 18th European Symposium on Improved Oil Recovery, EAGE, Dresden, Germany, 14-16 April*.
25. Firoozabadi, A. (2000). Recovery mechanisms in fractured reservoirs and field performance. *Journal of Canadian Petroleum Technology*, *39*(11).
26. Fischer, H. and N. R. Morrow (2006) Scaling of oil recovery by spontaneous imbibition for wide variation in aqueous phase viscosity with glycerol as the viscosifying agent. *Journal of Petroleum Science and Engineering,* **52**, 35-53.
27. Hamidpour, E., Mirzaei-Paiaman, A., Masihi, M., & Harimi, B. (2015). Experimental study of some important factors on nonwetting phase recovery by cocurrent spontaneous imbibition. *Journal of Natural Gas Science and Engineering*, *27*, 1213-1228.
28. Haugen, Å., M. A. Fernø, G. Mason and N. R. Morrow (2014) Capillary pressure and relative permeability estimated from a single spontaneous imbibition test. *Journal of Petroleum Science and Engineering* **115**, 66-77.
29. Haugen, Å., Fernø, M. A., Mason, G., & Morrow, N. R. (2015). The effect of viscosity on relative permeabilities derived from spontaneous imbibition tests. *Transport in Porous Media*, **106**(2), 383-404.
30. Joonaki, E., Gahrooei, H. R. E., & Ghanaatian, S. (2016). Experimental study on adsorption and wettability alteration aspects of a new chemical using for enhanced oil recovery in carbonate oil reservoirs. *Journal of Unconventional Oil and Gas Resources*, **15**, 11-21.
31. Karimaie, H., Torsæter, O., Esfahani, M. R., Dadashpour, M., & Hashemi, S. M. (2006). Experimental investigation of oil recovery during water imbibition. *Journal of Petroleum Science and Engineering*, *52*(1-4), 297-304.
32. Li, Y., Ruth, D., Mason, G., & Morrow, N. R. (2006). Pressures acting in counter-current spontaneous imbibition. *Journal of Petroleum Science and Engineering*, **52**(1-4), 87-99.
33. Lohne, A. (2013). User's Manual for BugSim–an MEOR Simulator (V1. 2). Technical report, IRIS.
34. Mahani, H., Berg, S., Ilic, D., Bartels, W. B., & Joekar-Niasar, V. (2015). Kinetics of low-salinity-flooding effect. *SPE Journal*, **20**(01), 8-20.
35. Mason, G., H. Fischer, N. R. Morrow, D. W. Ruth and S. Wo (2009) Effect of sample shape on counter-current spontaneous imbibition production vs time curves. *Journal of Petroleum Science and Engineering,* **66**, 83-97.

36. Mason, G., & Morrow, N. R. (2013). Developments in spontaneous imbibition and possibilities for future work. *Journal of Petroleum Science and Engineering*, **110**, 268-293.
37. Mattax, C. C., & Kyte, J. R. (1962). Imbibition oil recovery from fractured, water-drive reservoir. *SPE Journal*, **2**(02), 177-184.
38. McPhee, C., Reed, J., & Zubizarreta, I. (2015). *Core analysis: a best practice guide* (Vol. 64). Elsevier.
39. Megawati, M., Hiorth, A., & Madland, M. V. (2013). The impact of surface charge on the mechanical behavior of high-porosity chalk. *Rock mechanics and rock engineering*, *46*(5), 1073-1090.
40. Meng, Q., Liu, H., Wang, J., & Zhang, H. (2016). Effect of wetting-phase viscosity on cocurrent spontaneous imbibition. *Energy & Fuels*, **30**(2), 835-843.
41. Meng, Q., Liu, H., & Wang, J. (2017). Effect of viscosity on oil production by cocurrent and countercurrent imbibition from cores with two ends open. *SPE Reservoir Evaluation & Engineering*, **20**(02), 251-259.
42. Morrow, N. R. and Xie, X. (2001). Oil Recovery By Spontaneous Imbibition From Weakly Water-Wet Rocks. *Petrophysics,* **42**(4).
43. Nazari Moghaddam, R., Bahramian, A., Fakhroueian, Z., Karimi, A., & Arya, S. (2015). Comparative study of using nanoparticles for enhanced oil recovery: wettability alteration of carbonate rocks. *Energy & Fuels*, **29**(4), 2111-2119.
44. Pooladi-Darvish, M., & Firoozabadi, A. (2000). Cocurrent and countercurrent imbibition in a water-wet matrix block. *Spe Journal*, *5*(01), 3-11.
45. Qiao, C., Li, L., Johns, R. T. et al. (2014). A mechanistic model for wettability alteration by chemically tuned water flooding in carbonate reservoirs. Presented at the SPE annual technical conference and exhibition, Amsterdam, the Netherlands, 27-29 Oct.
46. Qiao, Y., Andersen, P. Ø., Evje, S., & Standnes, D. C. (2018). A mixture theory approach to model co-and counter-current two-phase flow in porous media accounting for viscous coupling. *Advances in water resources*, **112**, 170-188.
47. RezaeiDoust, A., Puntervold, T., Strand, S., & Austad, T. (2009). Smart water as wettability modifier in carbonate and sandstone: A discussion of similarities/differences in the chemical mechanisms. *Energy & fuels*, **23**(9), 4479-4485.
48. Salathiel, R. A. (1973). Oil recovery by surface film drainage in mixed-wettability rocks. *Journal of Petroleum Technology*, *25*(10), 1-216.
49. Schechter, D. S., Zhou, D., & Orr Jr, F. M. (1994). Low IFT drainage and imbibition. *Journal of Petroleum Science and Engineering*, *11*(4), 283-300.
50. Schmid, K. S., Geiger, S., & Sorbie, K. S. (2011). Semianalytical solutions for cocurrent and countercurrent imbibition and dispersion of solutes in immiscible two-phase flow. *Water Resources Research*, **47**(2).
51. Seyyedi, M., Sohrabi, M., & Farzaneh, A. (2015). Investigation of rock wettability alteration by carbonated water through contact angle measurements. *Energy & Fuels*, **29**(9), 5544-5553.
52. Standnes, D. C., & Austad, T. (2000). Wettability alteration in chalk: 2. Mechanism for wettability alteration from oil-wet to water-wet using surfactants. *Journal of Petroleum Science and Engineering*, *28*(3), 123-143.
53. Standnes, D. C. (2004). Experimental study of the impact of boundary conditions on oil recovery by co-current and counter-current spontaneous imbibition. *Energy & fuels*, *18*(1), 271-282.
54. Standnes, D. C., Evje, S., & Andersen, P. Ø. (2017). A novel relative permeability model based on mixture theory approach accounting for solid–fluid and fluid–fluid interactions. *Transport in Porous Media*, **119**(3), 707-738.

55. Standnes, D. C., & Andersen, P. Ø. (2017). Analysis of the impact of fluid viscosities on the rate of countercurrent spontaneous imbibition. *Energy & fuels*, **31**(7), 6928-6940.
56. Stoll, M., Hofman, J., Ligthelm, D. J., Faber, M. J., & van den Hoek, P. (2008). Toward field-scale wettability modification—the limitations of diffusive transport. *SPE Reservoir Evaluation & Engineering*, **11**(03), 633-640.
57. Strand, S., Standnes, D. C., and Austad, T. (2006). New wettability test for chalk based on chromatographic separation of SCN- and SO42-. *Journal of Petroleum Science and Engineering*, *52*, 187-197.
58. Suleimanov, B. A., Ismailov, F. S., & Veliyev, E. F. (2011). Nanofluid for enhanced oil recovery. *Journal of Petroleum Science and Engineering*, **78**(2), 431-437.
59. Unsal, E., Mason, G., Morrow, N. R., & Ruth, D. W. (2007). Co-current and counter-current imbibition in independent tubes of non-axisymmetric geometry. *Journal of colloid and interface science*, **306**(1), 105-117.
60. Washburn, E. W. (1921). The dynamics of capillary flow. *Physical review*, *17*(3), 273.
61. Xie, Q., Liu, F., Chen, Y., Yang, H., Saeedi, A., & Hossain, M. M. (2019). Effect of electrical double layer and ion exchange on low salinity EOR in a pH controlled system. *Journal of Petroleum Science and Engineering*, **174**, 418-424.
62. Zhou, X., Morrow, N. R., & Ma, S. (2000). Interrelationship of wettability, initial water saturation, aging time, and oil recovery by spontaneous imbibition and waterflooding. *SPE Journal*, **5**(02), 199-207.
63. Zhou, D., Jia, L., Kamath, J. et al. (2002). Scaling of counter-current imbibition processes in low-permeability porous media. *Journal of Petroleum Science and Engineering*, *33*, 61-74.